

Lifespan Prediction and Multiobjective Optimization of Electrical Submersible Pump Wells Using Machine Learning

XingYuan Liang¹ , Xin Lu^{1*}, GuoQing Han¹ , He Zhang², KeGang Ling³, and LuTing Wang⁴

¹Institute of Petroleum Engineering, China University of Petroleum, Beijing, China

²Ryder Scott Company, L.P., Houston, Texas, USA

³University of North Dakota, Grand Forks, North Dakota, United States

⁴Institute of Mechanics, Chinese Academy of Sciences, Beijing, China

Summary

To enhance the lifespan of electrical submersible pumps (ESPs) and identify key influencing factors, we develop a survival-informed deep learning framework that combines Cox proportional hazards (CPH) analysis with a long short-term memory (LSTM) network for remaining life prediction. A multiobjective optimization model based on the version 2 nondominated sorting genetic algorithm (NSGA-II) is further introduced to balance lifespan and production. A distinctive feature of the proposed framework is its integration of survival analysis, deep learning, and multiobjective optimization into a single methodology, enabling both accurate lifespan prediction and practical operational optimization. Field applications show that it outperforms contemporary deep learning baselines, achieving a magnitude of relative error (MRE) of 0.23, mean absolute error (MAE) of 0.05, and root mean squared error (RMSE) of 0.065 on the test set. In a field validation involving 30 ESP wells over a 1-year evaluation period, the proposed multiobjective optimization achieved up to 20.3% higher cumulative production compared with single-objective optimization, while maintaining a comparable average lifespan. These results demonstrate both predictive accuracy and significant operational value.

Introduction

Artificial lift is crucial for oil fields worldwide. Using several artificial lift methods can prolong the life of wells and increase oil recovery. One of the most commonly used artificial lift methods is ESP. About 15–20% of the world's one million wells use ESPs due to their ability to produce high rates in deep wells (Pham et al. 2021). ESP wells account for approximately 60% of annual global crude oil production (Sobhy et al. 2025), and ESPs account for 43% of global yearly artificial lift costs (Yang et al. 2022). The performance and lifespan of ESPs in oil fields can be affected by various issues such as a mismatch between the formation's supply capacity and the capability of the ESP, the high temperature at the pump inlet, current fluctuation of the submersible electrical motor (SEM), making frequent adjustments to the frequency, and high gas/liquid ratio fluids. Oilfield benefits are highly correlated with the lifespans of ESPs. A shorter ESP lifespan can lead to increased maintenance costs and decreased production. To stabilize the operation of ESPs and extend their service lives, a reliable method is required to determine how different operations and conditions affect ESP lifespan and predict its remaining life.

At present, the methods for analyzing the survival of ESPs and the factors affecting them can be broadly classified into traditional and machine learning methods. Among them, the traditional method refers to using a large amount of historical data and statistical means to analyze an ESP's stability and maintenance time. The earliest study by Patterson (1993) presents a mathematical model to estimate the life expectancy of an ESP. Patterson utilized a statistical technique called the "Poisson pure death process" to determine the probability of system failure using sparse data. This method required only one parameter and was applied to ESP failure data from an oil field in west Texas. Recently, Al-Ballam et al. (2022) developed a statistical method to diagnose and assess the underlying reasons for ESP failures. Their approach was based on field data collected over 5 years from 10 wells. A Weibull statistical analysis model was created to evaluate the reliability characteristics and estimate the probability of ESP failure. Operators can perform preventive maintenance using this model to reduce the likelihood of failures. In addition to assessing the lifespan of an ESP, scholars have attempted to find ways to extend it through statistical analysis or historical data analysis. Al-Sadah (2014) conducted data analysis to determine the leading causes of ESP failure. Al-Sadah implemented dismantle inspection and failure analysis procedures to improve ESP run life. Borling et al. (2008) drew on experience from 13,176 ESP system cases in TNK-BP to optimize equipment selection and installation procedures, resulting in improved ESP run life. Traditional methods offer simplicity but lack precision and comprehensiveness and fail to capture nonlinear relationships and interactions between variables that affect ESP performance. With the continuous advancement of machine learning technologies and computational power, experts and scholars are increasingly using neural networks for more accurate ESP lifespan prediction.

In a study conducted by Melo et al. (2023), the authors explored the combination of machine learning techniques and physically-based damage modeling to create an automated real-time prediction system for the remaining useful life of an ESP. This system can provide alerts when an ESP is likely to fail within the next 90 days. However, the research relies primarily on synthetic data sets generated by digital twins for model training and testing, which may not fully capture the complexity and diversity of operational data in the field. Alam et al. (2020) utilized an autoencoder trained on a 2-year historical data dump from 97 sensors to detect anomalous behavior in an ESP and determine the root cause of an anomalous event. However, this study did not mention how to optimize for anomalous behavior. Al Radhi et al. (2021) presented a study by Abu Dhabi National Oil Company in collaboration with nybl, a deep tech development company, to predict ESP failures and lifespan using three different machine learning models—Failure Prediction Index, Remaining Run Life, and Virtual Flow Meter. Furthermore, productivity and ESP lifespan are improved by optimizing operation and scheduling. The machine learning techniques mentioned above are very precise and can analyze complex and nonlinear relationships between various factors that

*Corresponding author; email: luxincup@outlook.com

Copyright © 2026 Society of Petroleum Engineers

This paper (SPE 221041) was accepted for presentation at the SPE Annual Technical Conference and Exhibition, New Orleans, Louisiana, USA, 23–25 September 2024, and revised for publication. Original manuscript received for review 25 July 2025. Revised manuscript received for review 20 November 2025. Paper peer approved 1 December 2025.

can impact the survival of ESP. Nevertheless, they face a challenge known as the “black box” problem. This implies that clarifying the reasons behind the model’s predictions is challenging.

Recent years have also witnessed significant progress in predictive analytics across related industrial domains, including turbines, compressors, and generators. In these areas, both statistical models and advanced machine learning algorithms—such as attention-based networks, ensemble learning, and graph neural networks—have been successfully applied for failure prediction and run-life estimation (Xiao et al. 2023; Ture et al. 2024; Lee et al. 2025; Forbicini et al. 2025). These advances highlight the maturity of predictive analytics for general industrial equipment, in contrast with the relatively limited development observed in ESP research. At the same time, recent studies on oilwell applications have begun to explore more sophisticated approaches, including transformer architectures, physics-informed models, and hybrid statistical-machine learning frameworks (Azmi et al. 2024; Zhu et al. 2025; Al Sawafi et al. 2024; Peng et al. 2025). Compared with traditional ESP analysis, these methods offer enhanced adaptability, improved interpretability, and better handling of nonlinear operating conditions. This contrast underscores the need for further advancement of predictive analytics in ESPs, justifying the integrated approach proposed in this study.

However, most existing ESP studies still focus on either lifespan prediction or production optimization in isolation, often relying on black-box models that lack interpretability and adaptability across different field conditions. Few approaches integrate survival analysis with deep learning to capture both the statistical reliability of ESPs and the temporal dynamics of operating data. Moreover, multiobjective optimization frameworks that jointly consider lifespan extension and production improvement remain scarce. This gap underscores the need for an integrated framework that combines interpretable survival modeling, sequence-based learning, and multiobjective optimization—precisely the direction pursued in this study.

Therefore, in this work we introduce a novel framework for dynamic survival analysis and lifespan prediction of ESPs. The approach integrates CPH modeling with an LSTM network, combining statistical interpretability with temporal sequence learning. A multiobjective optimization scheme based on NSGA-II is further incorporated to jointly extend ESP lifespan and enhance production. The main innovation lies in unifying survival analysis, deep learning, and multiobjective optimization into a single framework, which has not been previously applied to ESP management. Field application results show that the method achieves accurate lifespan prediction, quantifies key influencing factors, and translates optimization results into practical operational adjustments. By combining predictive accuracy with operational adaptability, the framework reduces unplanned interventions, improves production efficiency, and provides a new pathway for intelligent ESP management.

Models and Methods

Fig. 1 illustrates the main steps of the dynamic survival analysis and lifespan prediction method for ESP based on the fusion of the CPH model and LSTM network.

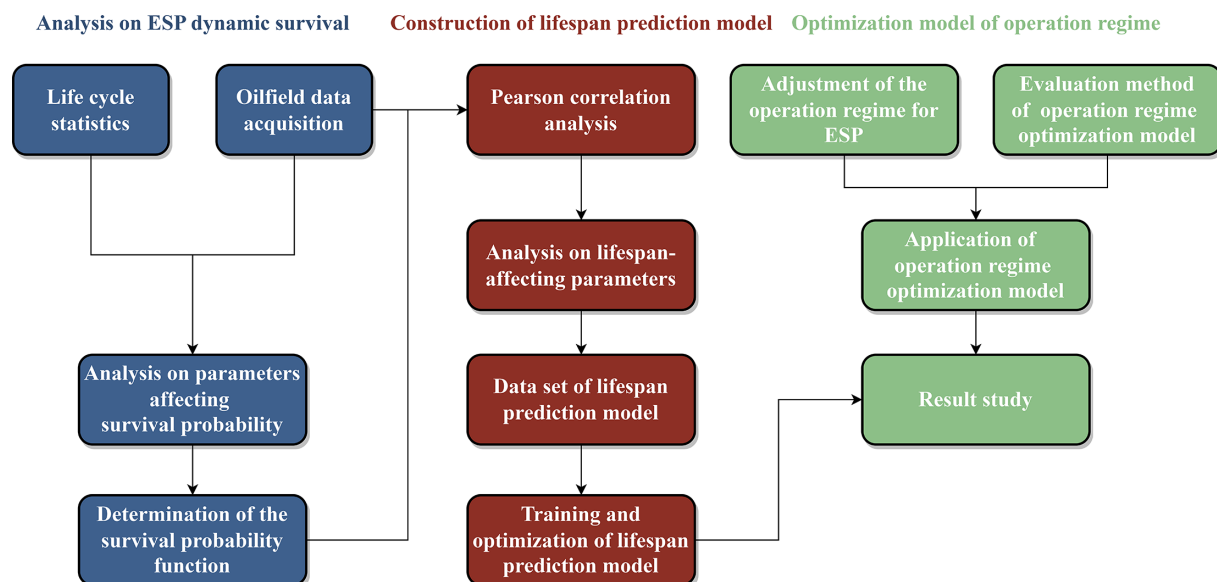


Fig. 1—Process of ESP dynamical survival analysis and lifespan prediction.

Step 1. Acquire and process data, then quantify the impact of each parameter on the probability of survival and ultimately build a survival probability function.

Step 2. Construct the data set for ESP lifespan prediction modeling by retaining the parameters with a strong correlation to lifespan and eliminating those with minimal impact. Divide the data set into training, validation, and test sets.

Step 3. Train the LSTM model on the training set, find the optimal hyperparameters on the validation set, and evaluate the prediction effect on the test set.

Step 4. Analyze historical data of the ESP system to establish an operating regime adjustment scheme according to parameters affecting survival probability obtained in Step 1.

Step 5. Based on the established operating regime adjustment scheme in Step 4, the lifespan prediction model was utilized for optimal adjustment selection to prolong the lifespan of ESP.

Survival Analysis of ESP. The survival analysis of the ESPs investigates the relationship between operating time, survival probability, and the impact of explanatory variables (EVs). The survival probability function, used for lifespan prediction and production optimization, was established from wellhead and downhole data of 712 ESP wells in a Chinese offshore oil field, with the corresponding data summarized

in **Table 1**. The production data set covers wells operating under diverse reservoir and operating conditions to enhance the model's generalization capability. The data set spans Years 2015–2023, with wellhead parameters (e.g., tubinghead pressure, casing pressure, motor current, and frequency) recorded hourly and downhole measurements (e.g., pump intake pressure and motor temperature) every 10 minutes. Wells were operated under multiple control strategies, including fixed-frequency, closed-loop proportional-integral-derivative, and intermittent regimes, and both mean and standard deviation values of EVs were incorporated to capture fluctuations under intermittent operation. Another important factor affecting ESP lifespan is the deviation of the operating point from the rated condition on the head/flow curve. Because the curve may shift dynamically with operating conditions and time and may even lose validity under abnormal states such as gas lock or cavitation, an explicit head/flow deviation index was not incorporated. Instead, EVs such as flow rate, motor current, and intake/discharge pressure provide indirect indications of this deviation. In addition to these regular control regimes, field records show that some ESPs were temporarily shifted to very low frequency operation during emergency conditions, particularly to mitigate extreme overheating. In this context, the minimum frequency reported in **Table 1** (21 Hz) corresponds to such short-term protective operation and is therefore not considered an outlier but rather a safeguard occasionally used in practice.

No.	Variable Symbol	Influencing Factors	Unit	Minimum	Mean	Maximum
1	V1	Tubinghead pressure	psi	153.15	289.61	665.51
2	V2	Casing pressure	psi	100.05	247.39	630.52
3	V3	Pump inlet pressure	psi	103.07	454.49	1,932.4
4	V4	Pump outlet pressure	psi	252	1,568.96	2,000
5	V5	Pump inlet temperature	°C	40.21	58.83	79.91
6	V6	Motor temperature	°C	40.07	89.55	139.29
7	V7	Current	A	15.39	44.52	82.89
8	V8	Voltage	V	609.02	1,840.84	2,536.1
9	V9	Frequency	Hz	21	49.36	65.67
10	V10	Motor power	kW	13.87	104.96	250.00
11	V11	Oil	BOPD	3.69	429.02	1,486.68
12	V12	Gas	Mscf/D	1.05	139.95	972.41
13	V13	Water	BOPD	1.06	1,495.92	7,997.41
14	V14	Liquid	BOPD	16.72	1,928.17	9,188.45
15	V15	Gas/oil ratio	Mscf/bbl	0.01	0.32	1.86

Table 1—Basic overview of 712 ESP wells in an offshore oil field in China.

Although systematic field records of complicating factors such as scale deposition, gas content, asphaltene/resin/paraffin deposits, and abrasive particles were not available, this absence reflects limitations in site documentation rather than their irrelevance. Their effects are indirectly captured through operating parameters—for instance, fluctuations in motor current, frequency changes, or pump intake pressure variations—ensuring that these influences are still incorporated into the survival analysis. Preprocessing included imputing missing values via grey adaptive K-nearest neighbor, removing outliers with Chauvenet's criterion, and normalizing all variables before model construction, ensuring comparability across coefficients and avoiding physically meaningless baseline conditions.

These data include ESPs that are still functioning and ESPs that have failed. It is important to note that functioning ESPs represent right-censored data, which is a critical concept in survival analysis. Right-censored data (Klein and Moeschberger 2003) occurs when the observation period ends before an event has occurred. In the case of ESP, pumps still functioning at the end of the observation period have yet to fail, but they could fail in the future. The key variables and their statistical ranges used for survival modeling are summarized in **Table 1**. Including these censored data points provides essential information on the minimum lifespan of these pumps, which, in turn, helps in estimating the survival probability function more accurately. **Fig. 2** provides a visual representation of the right-hand censoring utilized in this study.

Determination of Survival Probability Function. For this study, we used the CPH model to determine the survival probability function. The CPH model is a semiparametric regression model proposed by Cox (1972). The model is typically used in medical research to analyze the effect of one or more predetermined variables on a patient's survival time. In particular, the CPH model was chosen because it can incorporate multiple EVs to quantify how operating parameters influence ESP lifespan. Its semiparametric form avoids strict assumptions on the baseline hazard, ensuring adaptability to diverse field conditions. It also yields interpretable hazard ratios for practical decision-making. Unlike parametric models such as Weibull, which require a predefined hazard shape, or nonparametric methods such as Kaplan-Meier, which cannot handle multiple covariates, the CPH model provides a flexible and interpretable framework well-suited for heterogeneous offshore oilfield data. The CPH model can be written as follows:

$$h(t, X) = h_0(t) \exp \left(\sum_{i=1}^n \beta_i x_i \right), \quad (1)$$

where $h(t, X)$ is the expected hazard at time t and $h_0(t)$ is the baseline hazard function that represents the hazard when all of the EVs $X = \{x_1, x_2, \dots, x_n\}$ are equal to zero. $\beta = \{\beta_1, \beta_2, \dots, \beta_n\}$ are the coefficients of the EVs that measure the impact of each EV on the hazard. The model parameters are estimated by maximizing a likelihood expression that does not contain the baseline hazard function, while the baseline hazard function is estimated nonparametrically. Note in Eq. 1 that the baseline hazard function involves time t but not X . The effects of EVs are additive on the log-hazard scale; however, when multiple variables deviate from the baseline simultaneously, their joint contribution is incorporated through the exponential transformation, so the hazard ratio can be amplified or attenuated beyond a simple linear addition. The standard CPH model, therefore, does not explicitly capture more complex nonlinear interactions, which are further

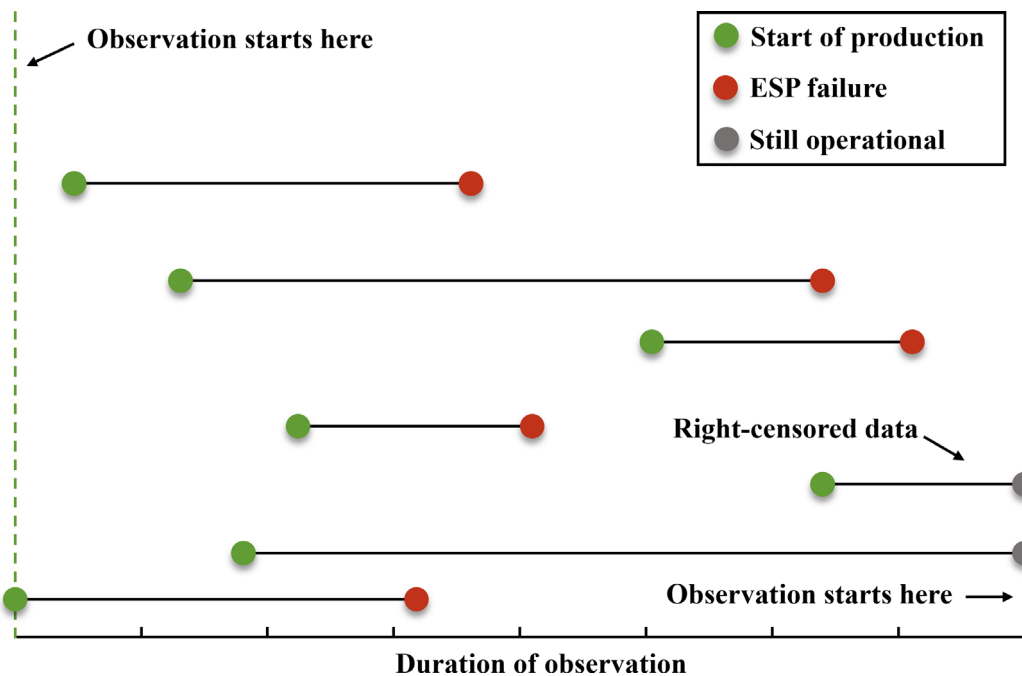


Fig. 2—Illustration of right-censored data in ESP survival analysis, where green dots indicate the start of production, red dots represent ESP failure, and gray dots denote units still operational at the end of observation. Horizontal lines show the observed lifetime, with right-censored cases occurring when failure has not been observed within the study period.

explored in subsequent modeling stages using advanced learning methods to complement the CPH framework. The survival probability function can be derived from the hazard function, which can be written as follows:

$$S(t, X) = \exp(-H(t, X)), \quad (2)$$

where $H(t, X)$ is the integral of the hazard function $h(t, X)$ from zero to t . The baseline survival function $S_0(t, X)$ is obtained when all EVs are taken to be zero. The survival function expresses the probability of an individual surviving over a certain period. On the other hand, the hazard function provides the probability of an event happening to an individual at any given time. We can analyze and interpret data from various perspectives by examining these functions and their interplay.

Another essential concept is the hazards ratio (HR), which is the ratio of the hazard associated with one set of EVs to the hazard associated with another set of EVs. Thus:

$$HR = \frac{h_0(t) \exp(\sum_{i=1}^n \beta_i x_i)}{h_0(t) \exp(\sum_{i=1}^n \beta_i x_i^*)} = \exp\left(\sum_{i=1}^n \beta_i (x_i - x_i^*)\right). \quad (3)$$

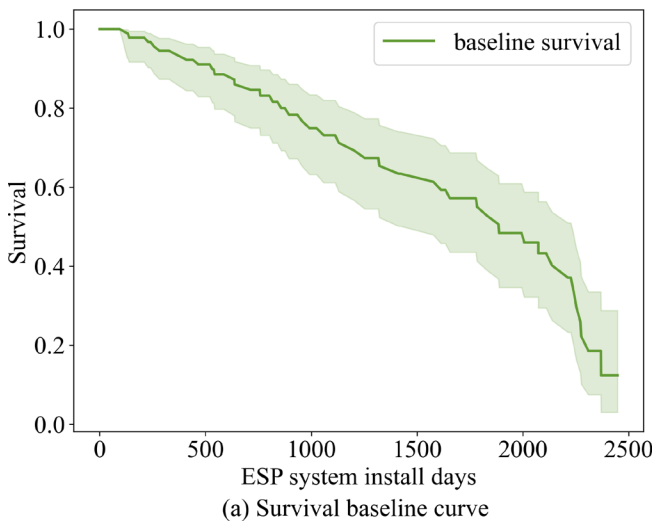
It can be inferred from the above equation that when HR is greater than unity, the individual's hazard represented by X is higher than that of the individual represented by X^* . Considering a simple model that includes only the EV x_1 , and two individuals, one of which takes x_1 to be zero and the other unity, then the HR of these two individuals can be written as follows:

$$HR = \exp(\beta_1 (x_1 - x_1^*)) = \exp(\beta_1 (1 - 0)) = \exp(\beta_1). \quad (4)$$

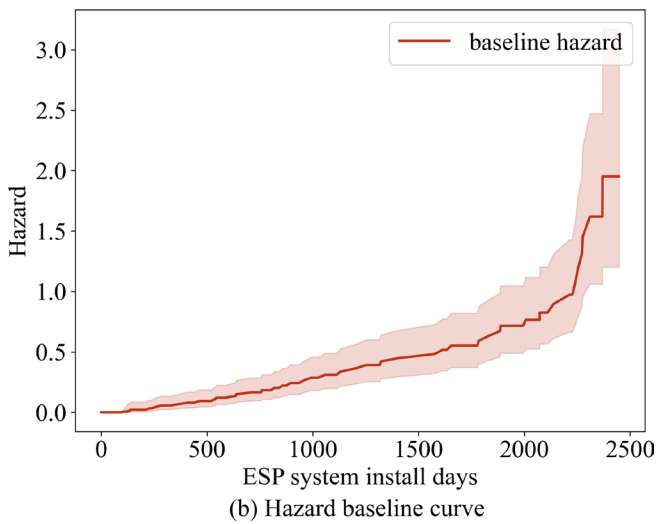
If the value of β is greater than zero, then the HR is greater than unity. This implies that the EV X_1 has a negative impact on the survival of the individual. On the other hand, if β is equal to zero, then the HR becomes unity, which shows that X_1 does not affect the survival of the individual. Finally, if β is less than zero, then the HR is less than unity, indicating that the X_1 has a positive effect on the survival of the individual.

In this study, we calculated the mean and standard deviation of the parameters at the wellhead and downhole for each individual ESP unit during the observation period and used them as EVs in the CPH model. Some diagnostic indicators such as insulation resistance, current imbalance, and voltage imbalance were not included because systematic field records of these parameters were not available. Moreover, reliable estimation of imbalance requires high-frequency three-phase acquisition, which would generate extremely large data sets and substantially increase the computational cost of model training. Nevertheless, related EVs such as motor current, motor temperature, and frequency fluctuations can indirectly reflect abnormalities in motor loading and electrical conditions, thereby partially capturing the effects of these diagnostic indicators. After the model fitting, the proportional hazards assumption was assessed using Schoenfeld residuals, and no evidence against the assumption was found ($p > 0.05$). The baseline survival and hazard curves illustrate the basic survival status. **Fig. 3** shows the baseline survival and hazard curves, respectively.

Fig. 4 shows the HR of EVs with 95% confidence intervals (CIs), where squares represent HR estimates and horizontal lines denote the CIs. Squares positioned above 1.0 indicate an estimated increase in risk, while squares below 1.0 indicate an estimated reduction in risk. When the 95% CI spans both sides of 1.0 (i.e., the lower bound is < 1.0 and the upper bound is > 1.0), the effect is not statistically significant; such cases are interpreted as indicative trends that require cautious interpretation in field practice. Most EVs negatively affect survival probability, while some, such as average liquid rate, pump inlet pressure, and pump outlet pressure, have a positive impact. This



(a) Survival baseline curve



(b) Hazard baseline curve

Fig. 3—Baseline survival and hazard curves of the ESP system: (a) Baseline survival curve showing the probability of the ESP remaining operational over time with confidence intervals and (b) baseline hazard curve illustrating the increasing risk of failure as installation days progress.

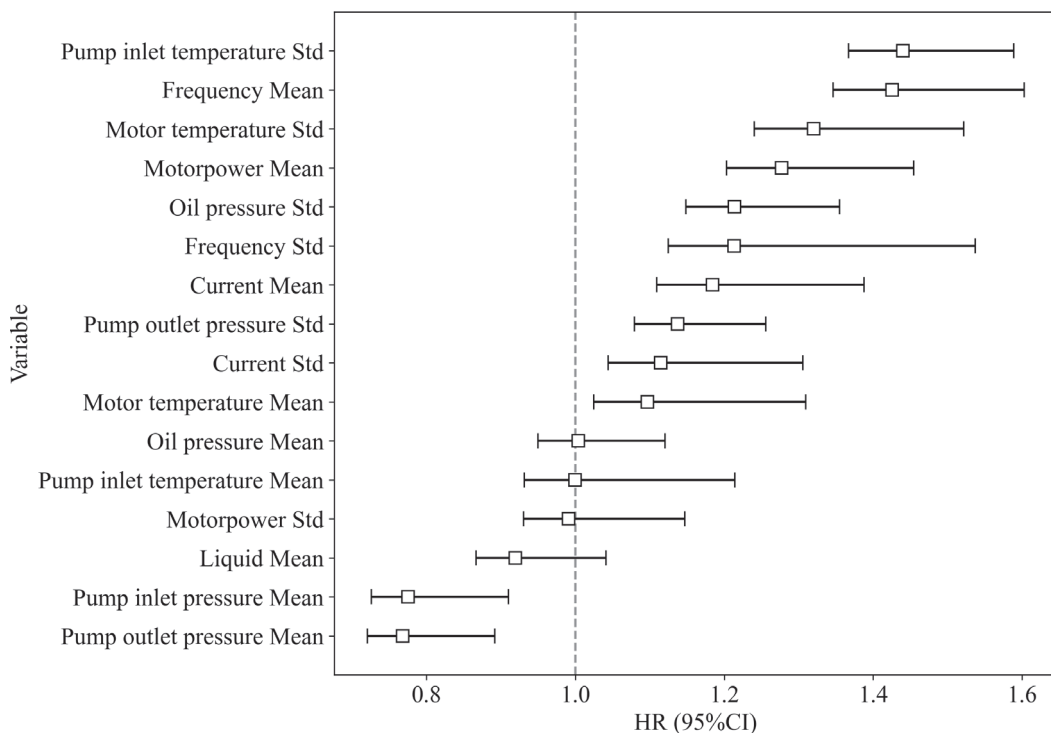


Fig. 4—HRs with 95% CIs for different EVs in the CPH model, where values above 1.0 indicate an increased risk of ESP failure and values below 1.0 indicate a reduced risk.

positive effect reflects the physical operating context: ESP capacity in the studied offshore oil field generally exceeds formation supply capacity, so higher liquid rate and inlet pressure better match the system and extend ESP service life.

Survival Analysis under the Influence of Different EVs. Once the survival probability function has been determined, it is possible to analyze the effect of different variables on survival. Splitting samples into groups based on certain characteristics and comparing survival curves between them can help identify the survival of specific subgroups, which can be a vital guide for parameter selection and equipment purchase.

Fig. 5 shows the comparison of the survival function for different frequency means, motor temperature means, current means, and motor power means. These four EVs have the most significant impact on the survival probability among the mean EVs. All four variables reflect the operating status of the motor, which indicates that the SEM's operating condition plays a crucial role in the lifespan of the ESP production system. The percentage of failure caused by ESPs in oil fields supports this conclusion. More than 60% of all failed ESP systems were due to motor or cable failures. The case presented here corresponds to wells with relatively long service life, which makes it possible to display the complete lifecycle behavior of the system and provide a representative picture of how survival probability evolves over the entire operating span. The larger these four EVs, the lower the probability of survival of the ESP production system, which

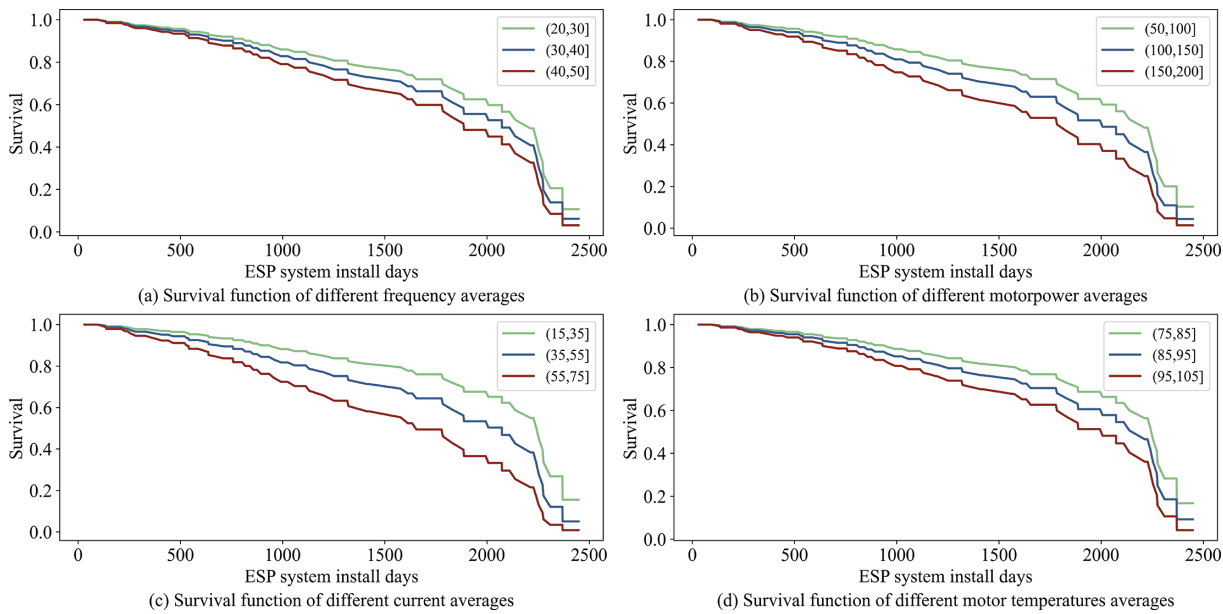


Fig. 5—Subgroup survival analysis with different mean EVs: (a) Survival function of different frequency averages; (b) survival function of different motor power averages; (c) survival function of different current averages; and (d) survival function of different motor temperature averages.

represents an increased risk of failure of the ESP production system if the SEM is under high load for an extended period during production. It is worth noting that the increase in the current mean led to a more significant reduction in survival probability compared with other EVs.

Therefore, greater attention should be paid to monitoring current changes during production. In most cases, if there is an increase in motor current while keeping the total power constant, it is usually attributed to various factors such as an increase in load, a decrease in motor efficiency, voltage fluctuation in power supply, and motor overheating. When the load of the ESP system increases, the frequency and nozzle can be adjusted to change the operating regime so that the motor is at the optimal operating point to avoid high current caused by motor overheating and reduced efficiency. Adding filters to the power supply can resolve voltage fluctuations. Filters remove unwanted noise and fluctuations, preventing damage to the electrical components of the motor and ensuring smooth system functioning.

Another set of comparisons concerns the standard deviation (std) EVs, as presented in Fig. 6. If the std EVs are higher, it indicates that the parameter is more unstable. The std EVs that have the greatest impact on survival probability are temperature, which includes inlet temperature std and motor temperature std. Temperature instability affects the density and viscosity of the fluid, which in turn affects the performance parameters of the ESP, such as displacement, head, and efficiency, leading to a deviation from the design value at the pump's operating point and a reduction in the pump's efficiency and performance. In addition, unstable temperatures can also lead to changes in thermal stresses in the pump's internal components, which may lead to problems such as deformation, cracking, or fatigue fracture of the components. Especially at high temperatures or sharp temperature changes, thermal stresses may seriously affect the reliability and safety of the pump. Another significant std EV is tubinghead pressure std. When the tubinghead pressure becomes unstable, it has a direct impact on the overall performance of the ESP. In addition, unstable tubinghead pressure can lead to a significant increase in the pump's vibration level, which can cause a host of other issues, such as heightened wear and tear, which can shorten its overall lifespan. The vibration can also affect the safety of the surrounding equipment, including separators and protectors, which can be particularly hazardous in certain situations. Frequency std also has a significant effect. The unstable operating frequency may lead to variations in motor loads, and frequent load variations may increase wear and tear and overheating of the motor, reducing its service life. Frequent starting and stopping of the ESP during production can also cause the frequency std to rise. The whole system is heavily loaded when starting and stopping, which accelerates equipment degradation. Especially during startup, the currents can be very high, which poses a significant risk of cable failures and additional energy consumption.

The CPH model analyzes not only the effect of a single EV on the probability of survival but also the effect of multiple EVs when they act synergistically. Fig. 7 compares the survival function for wells produced in high-frequency, low-liquid-rate, and low-frequency, high-liquid-rate cases. It can be seen that survival is better in cases of high liquid rate and low frequency. As mentioned above, the capacity of the ESP in an offshore oil field in China is generally greater than the supply capacity of the formation, and this mismatch makes the pumps work off the optimal point. While the high-liquid-rate, low-frequency case provides a better match, a higher probability of survival is also obtained.

Another set of multi-EV synergistic analyses (illustrated in Fig. 8) is on motor temperature mean and motor temperature std. High temperatures can have a significant impact on ESPs, but it is essential to determine which factor is more concerning—high temperatures or unstable temperatures. The curves in the figure demonstrate that despite operating at higher temperatures, it is still possible to achieve a better probability of survival if the temperature can be kept from fluctuating dramatically. This highlights the importance of maintaining stable temperatures in ESP to maximize their lifespan and ensure optimal performance.

Survival analyses not only find operating parameters that can maintain the ESP system within a high probability of survival but also make it possible to select the equipment manufacturer. Conducting a survival analysis of different subgroups categorized based on the manufacturers of ESPs and cable can help oilfield managers make informed decisions about which equipment is most reliable. This analysis can provide valuable insights into the durability and longevity of the equipment, helping ensure that it meets the necessary standards for use in various applications. The offshore oil field mentioned above uses ESPs from four manufacturers and cables from three manufacturers. It should be emphasized that the comparison was conducted for products of the same specification, so the differences reflect

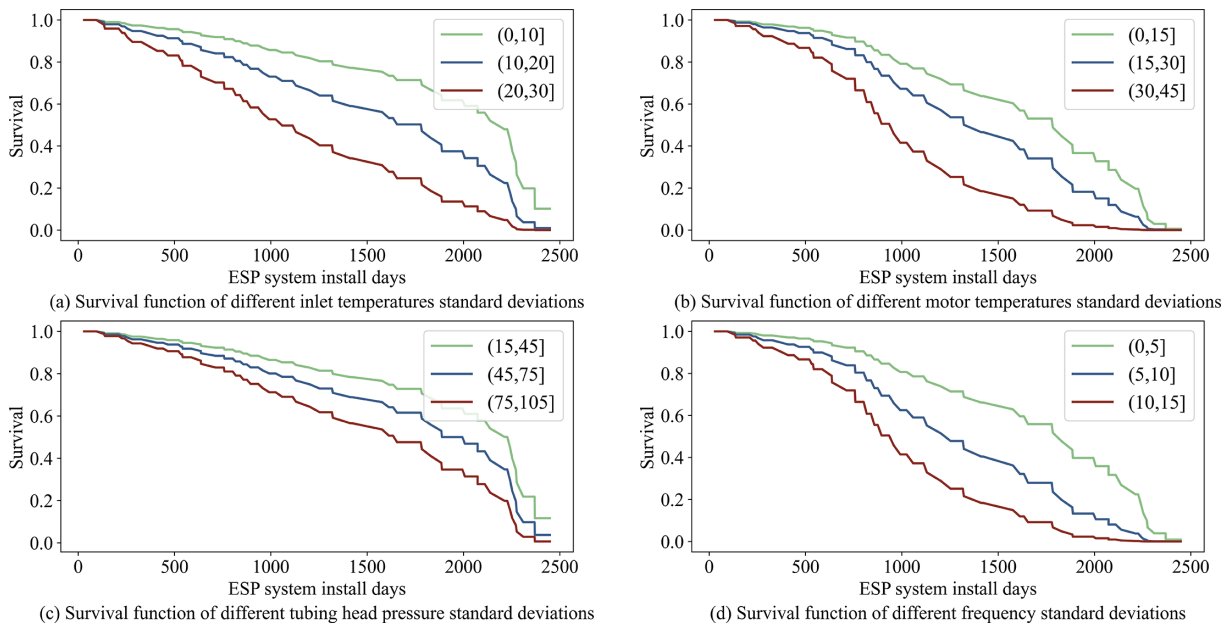


Fig. 6—Subgroup survival analysis with different stds of EVs: (a) survival function of different inlet temperature stds; (b) survival function of different motor temperature stds; (c) survival function of different tubinghead pressure stds; and (d) survival function of different frequency stds.

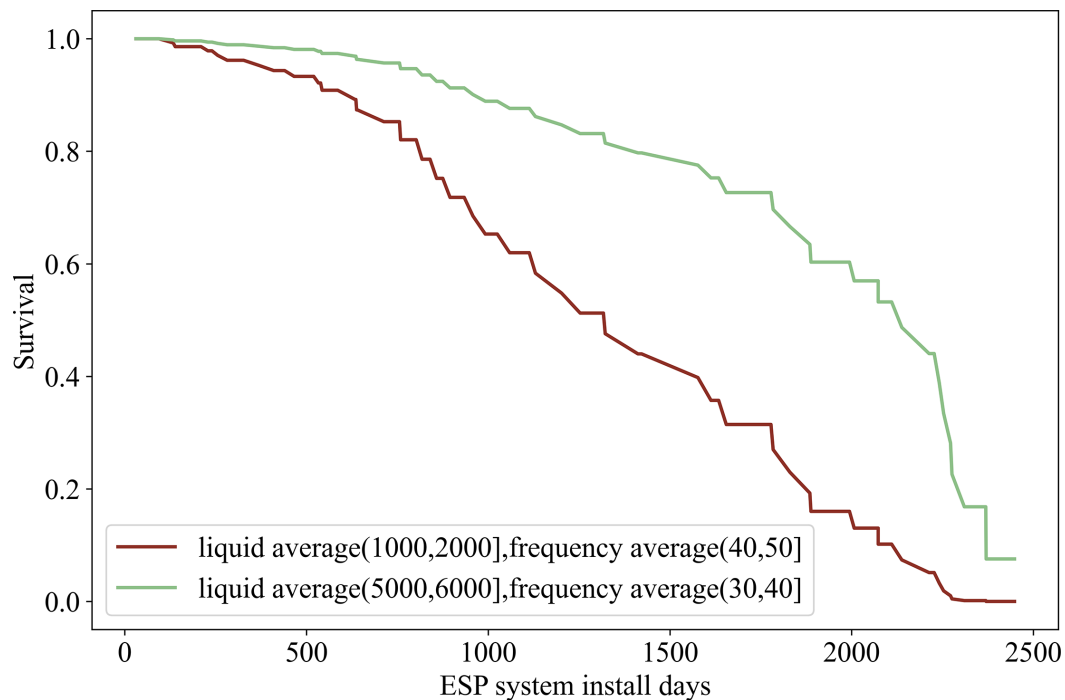


Fig. 7—Survival curves of ESP systems under different liquid rate-frequency combinations, showing improved survival in high-liquid-rate, low-frequency cases.

manufacturer-related factors rather than variations in design type or rated capacity. While these comparisons offer practical guidance, it should be recognized that deployment environments may differ among manufacturers, which could partly influence the observed outcomes. Therefore, the results should be interpreted with caution and considered in conjunction with operating conditions. Nevertheless, the survival curves for multiple combinations of ESP and cable manufacturers are shown in Fig. 9. It was observed that the best survival rate can be achieved by using an ESP from Manufacturer D along with a cable from Manufacturer A.

Lifespan Prediction Model and Performance Evaluation. To accurately predict the lifespan of ESPs in this study, we developed a prediction model using the LSTM algorithm, and compared the performances of the models trained with and without survival features to illustrate the necessity of survival analysis to improve the accuracy of lifespan prediction. Further, we adjusted the hyperparameters to select the best model for the subsequent optimization of the ESP operation regime.

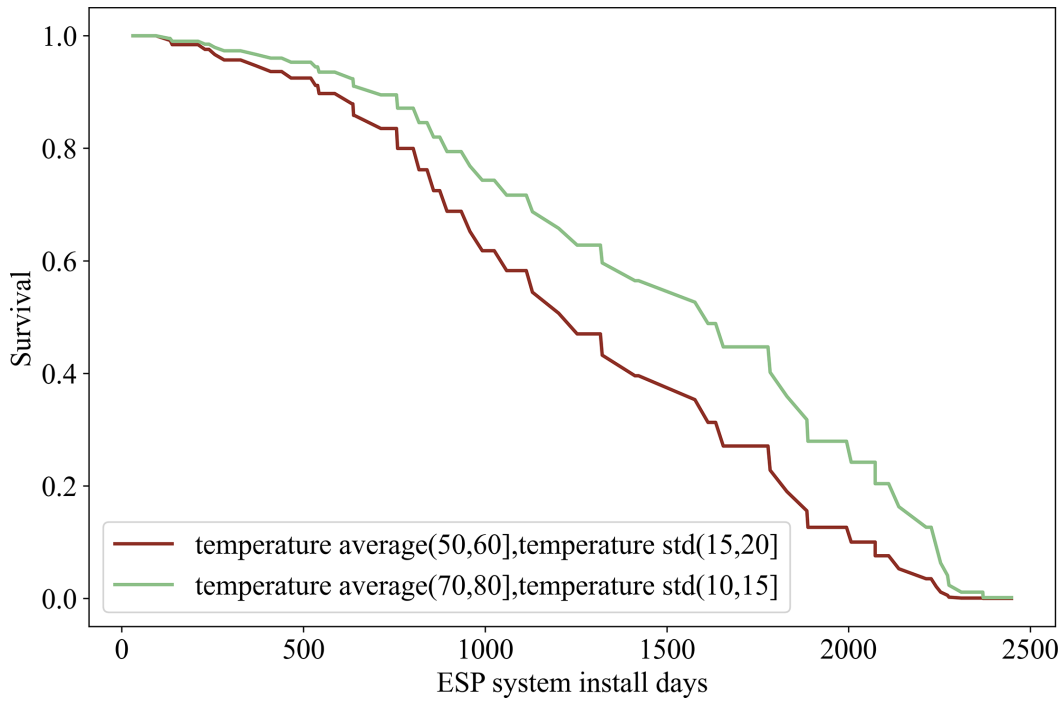


Fig. 8—Survival curves of ESP systems under different combinations of motor temperature mean and std illustrating that stable temperatures can mitigate the negative effects of higher average temperatures and improve survival probability.

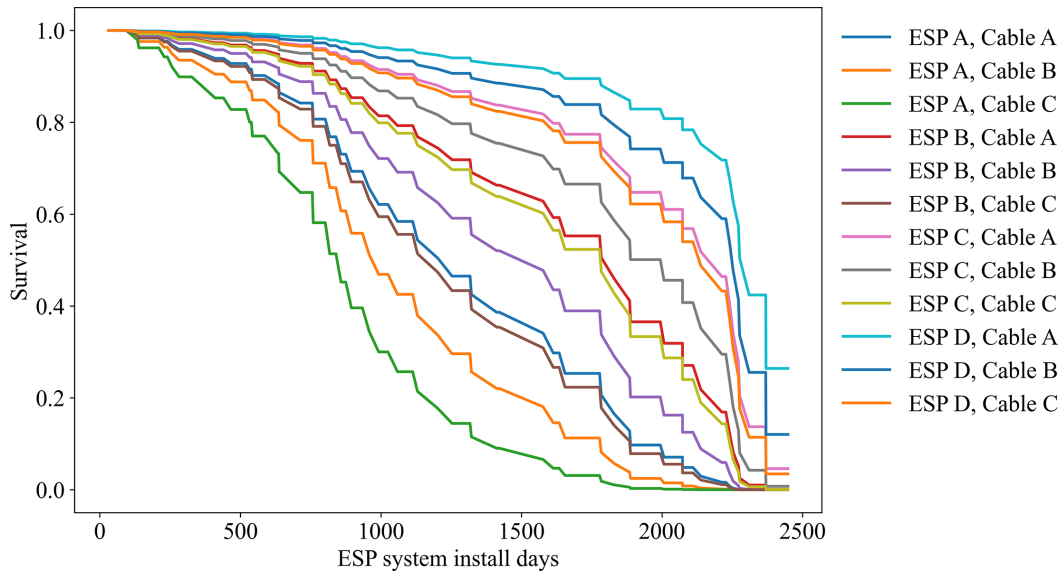


Fig. 9—Survival curves of ESP systems under different combinations of ESP and cable manufacturers, illustrating variations in equipment durability and showing that the best survival outcome is achieved with ESPs from Manufacturer D paired with cables from Manufacturer A.

Analysis of Lifespan Affecting Factors. For this study, we used the Pearson correlation coefficient method to determine the correlation between different variables and ESP lifespan. High-correlation variables were retained, while low-correlation variables were eliminated. The Pearson correlation coefficient ranges from -1 to 1 , with a stronger correlation having a higher absolute value. The Pearson correlation coefficient is calculated as follows:

$$r = \frac{\sum_{i=1}^n (X_i - \bar{X})(Y_i - \bar{Y})}{\sqrt{\sum_{i=1}^n (X_i - \bar{X})^2} \sqrt{\sum_{i=1}^n (Y_i - \bar{Y})^2}}, \quad (5)$$

where r represents the Pearson correlation coefficient, X_i and Y_i are the observed values of two variables, and \bar{X} and \bar{Y} are the averages of two variables. We used the Pearson coefficient method to analyze the correlation between 17 variables and the lifespan of 712 ESP wells in an offshore oil field in China. The results of the analysis are presented in Fig. 10 in the form of a heatmap. Of these 17 variables, 15 are demonstrated in Table 1. The remaining two variables are $h(t)$ and $T_{0.5}$. $h(t)$ is the survival probability function, providing the

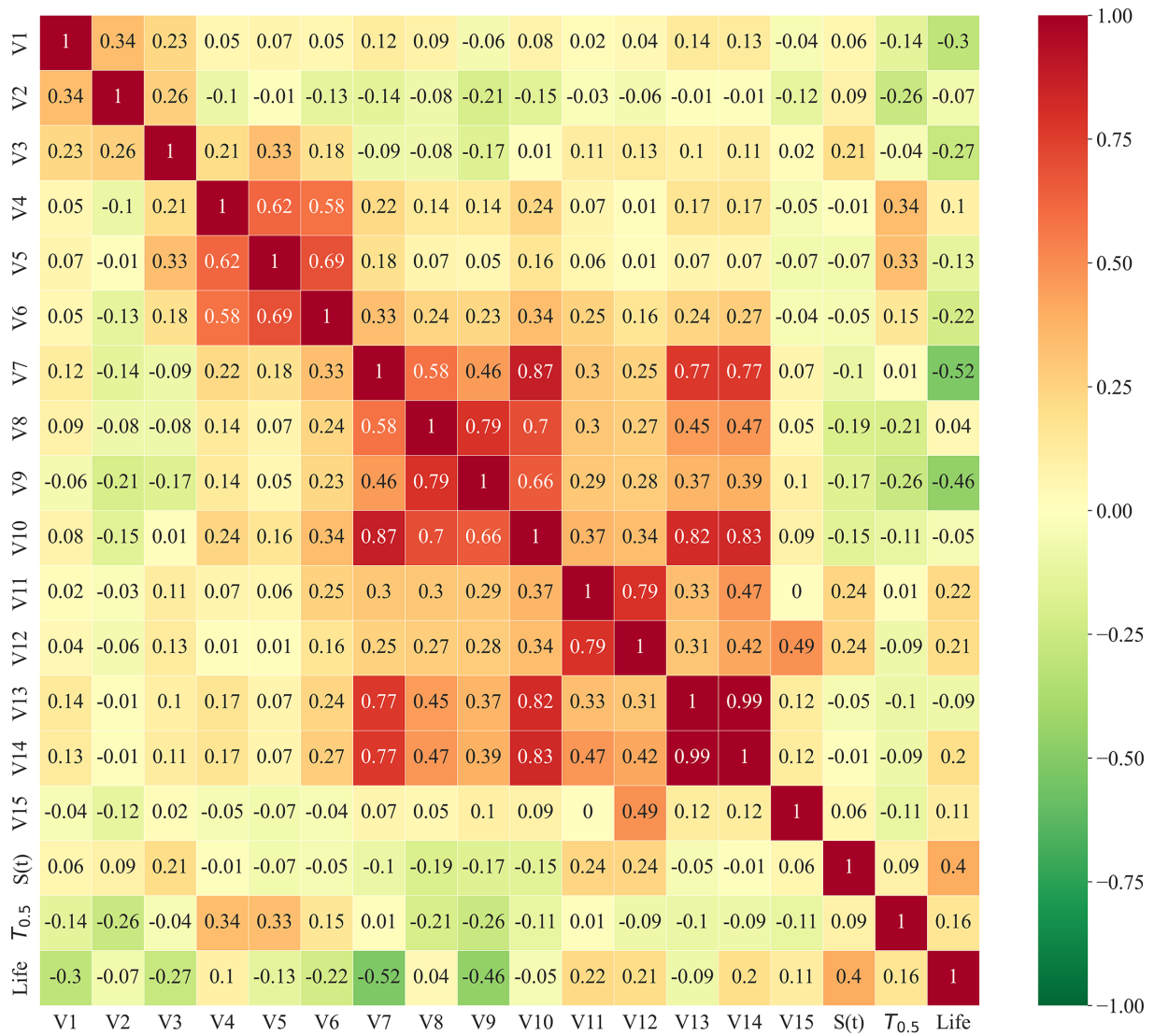


Fig. 10—Heatmap of Pearson correlation coefficients among 17 variables, showing strong correlations of ESP lifespan with operating current, frequency, and survival probability, and moderate correlations with pressure, temperature, and liquid rate.

survival probability of an ESP individual at time t , while $T_{0.5}$ is the median survival time (i.e., the ESP runtime when the survival probability is reduced to 0.5); the larger the value, the better the ESP would have survived. It can be seen from Fig. 10 that among the 17 lifespan influencing factors, ESP operating current, ESP operating frequency, and survival probability at time t are highly correlated with lifespan. Tubinghead pressure, pump inlet pressure, pump inlet temperature, motor temperature, oil rate, gas rate, liquid rate, gas/oil ratio, and median survival time are moderately correlated with lifespan. The above variables are identified as impacting ESP lifespan, and these variables will be used as input features for the lifespan prediction model to train the machine learning algorithm, while the rest will be eliminated. It should be noted that the Pearson correlation coefficient only captures linear dependencies and does not reflect potential nonlinear relationships. In this study, we used Pearson analysis as an initial screening tool for interpretability, while nonlinear influences were further captured in the subsequent LSTM-based modeling stage.

Pretraining and Optimization of Lifespan Prediction Model. We used the LSTM algorithm to create a model for predicting the lifespan of an ESP. LSTM is a trustworthy choice for predicting the ESP lifespan because of several advantages. First, LSTM solves the problem of capturing long-term dependencies present in sequential data, which is a common feature in time-series data sets like sensor readings from machinery. Unlike traditional models, LSTM networks incorporate memory cells and gating mechanisms, which allows them to retain information over extended periods, making it easier to model complex temporal patterns needed for ESP prediction. Second, ESP prediction often involves processing sequences of variable-length sensor measurements collected over time. LSTM's flexibility in handling sequences of varying lengths without requiring fixed-size input vectors makes it particularly well-suited for this task. This adaptability makes the model take into account irregular data sampling rates commonly encountered in the production environment of ESP systems, ensuring robust performance in oilfield applications. Third, real-time downhole or wellhead data often contain noisy or erroneous measurements, creating a challenge to traditional models. LSTM's robustness to noisy data allows it to effectively learn from imperfect information while filtering out irrelevant noise, ensuring accurate and reliable ESP lifespan predictions even in such imperfections. Using these strengths, LSTM-based models offer a powerful framework for predicting ESP lifespan. Fig. 11 illustrates the structure of the LSTM algorithm.

The LSTM algorithm involves a set of operations carried out at each timestep t . Let x_t represent the input at timestep t , h_t represents the hidden state, C_t represents the cell state, f_t represents the forget gate output, i_t represents the input gate output, and O_t represents the output gate output. The following equations govern the LSTM operations:

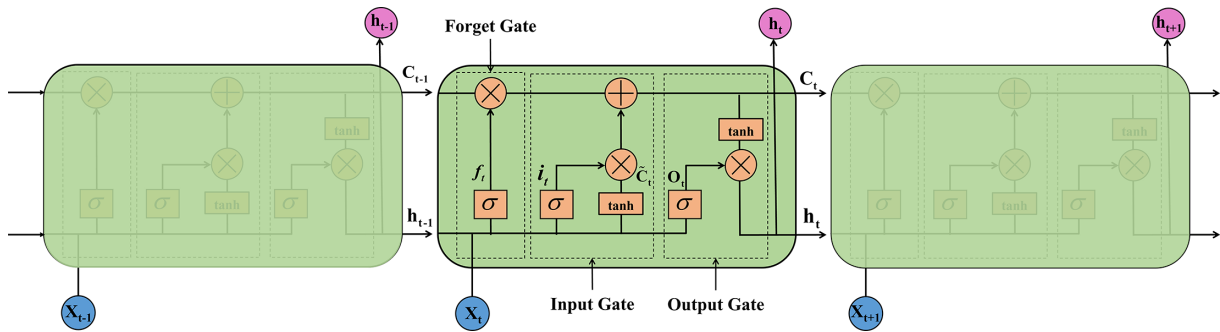


Fig. 11—Schematic representation of the LSTM architecture, showing the input, forget, and output gates that regulate information flow through the memory cell.

$$f_t = \sigma(W_f \cdot [h_{t-1}, x_t] + b_f), \quad (6)$$

$$i_t = \sigma(W_i \cdot [h_{t-1}, x_t] + b_i), \quad (7)$$

$$\tilde{C}_t = \tanh(W_c \cdot [h_{t-1}, x_t] + b_c), \quad (8)$$

$$C_t = f_t \cdot C_{t-1} + i_t \cdot \tilde{C}_t, \quad (9)$$

$$o_t = \sigma(W_o \cdot [h_{t-1}, x_t] + b_o), \quad (10)$$

$$h_t = o_t \cdot \tanh(C_t), \quad (11)$$

where W_f , W_i , W_c , and W_o represent weight matrices; b_f , b_i , b_c , and b_o represent bias vectors, and σ represents the sigmoid activation function.

Before we can pretrain the lifespan prediction model, we need to perform data windowing. Data windowing involves dividing time-series data into fixed-length subsequences for modeling purposes. By segmenting the data into windows, we can more effectively capture the temporal dependencies and patterns that are essential for accurate time-series prediction. However, choosing an appropriate window size can be challenging because a window that is too small may not capture long-term dependencies, while a window that is too large may result in computational inefficiency and information redundancy. In the case of lifespan prediction, we use features from T to $T + n - 1$ timesteps to predict the lifespan at timestep $T + n$, where n is the window length.

Twelve influencing factors were obtained from 712 sample wells, namely, tubinghead pressure, pump inlet pressure, pump inlet temperature, motor temperature, ESP operating current, ESP operating frequency, oil rate, gas rate, liquid rate, gas/oil ratio, survival probability at timestep t , and median survival time were used as model inputs, and ESP lifespan as model outputs to establish a prediction model using the LSTM algorithm. Sixty percent of the data set is split into a training set, 20% into a validation set, and 20% into a testing set. The training set is used to train the model, the validation set is used for hyperparameter tuning, and the testing set is used to evaluate the model's performance. To prevent data leakage and ensure fair model evaluation, the survival-analysis features (survival probability at timestep t and median survival time) were computed within each training fold only during cross-validation, using only the training data of that fold.

After completing the pretraining process, a preliminary evaluation of the model performance was performed. This study used three metrics to evaluate the prediction model's performance. The three evaluation metrics are the MRE, the MAE, and the RMSE, as demonstrated in **Table 2**.

Evaluation Metrics	Calculation Formula
MRE	$MRE = \sum_{i=1}^n \left \frac{y_t - y_{pre}}{y_t} \right \times \frac{1}{n}$
MAE	$MAE = \frac{\sum_{i=1}^n y_t - y_{pre} }{n}$
RMSE	$RMSE = \sqrt{\frac{1}{n} \sum_{i=1}^n (y_t - y_{pre})^2}$

Table 2—Lifespan prediction model evaluation metrics.

To support practical deployment, the computational requirements of the proposed model were evaluated. Model training was conducted on an NVIDIA Tesla V100 graphics processing unit (GPU) with 32 GB memory, and the training process typically required less than two hours for the full data set of 712 wells. Once trained, the inference and optimization modules can run on standard central processing unit-based servers without GPU acceleration. The average execution time for lifespan prediction and optimization per well is below 10 seconds, ensuring that the approach meets the requirements for near real-time field application. The final network architecture consisted of two stacked LSTM layers with 128 hidden units each, followed by fully connected layers for regression output. The LSTM model was trained with a batch size of 64 and up to 500 epochs, with early stopping applied based on validation loss to avoid overfitting. Dropout layers were incorporated to enhance robustness, and the Adam optimizer with a learning rate of 0.01 was used. Convergence of

the loss function was observed during training, confirming the correctness of the optimization process and stable generalization to unseen well data.

Fig. 12 displays the results of evaluating the lifetime prediction model that employs the LSTM algorithm. The pretrained model demonstrates an MRE of 0.26, MAE of 0.05, and RMSE of 0.06 on the training set. The MRE, MAE, and RMSE on the test set are 0.20, 0.05, and 0.07, respectively. Additionally, in this study we compare the error of the prediction model when survival analysis features are not included in the training vs. when they are included. The results show that incorporating survival analysis features reduces MRE by 48.9%, MAE by 37.5%, and RMSE by 40.9%, demonstrating that the LSTM algorithm is shown to improve the prediction model's accuracy by learning more patterns from the survival analysis features.

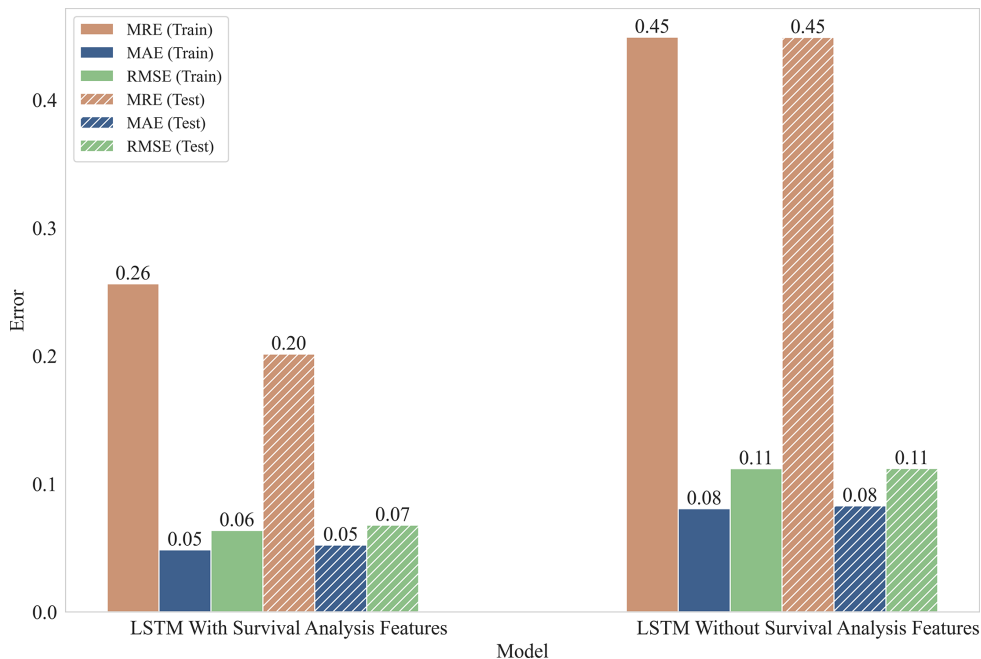


Fig. 12—Results of model evaluation showing that incorporating survival analysis features into the LSTM significantly reduces MRE, MAE, and RMSE compared with models without these features.

To further benchmark the proposed method, we compared the Cox + LSTM framework with several widely used machine learning and deep learning models, including random forest, gradient boosting decision tree, XGBoost, and temporal convolutional network. The comparative results are summarized in **Table 3**. As shown, the Cox + LSTM model consistently achieved the best performance across all evaluation metrics, with an MRE of 0.32, MAE of 0.037, and RMSE of 0.055. These values correspond to the cross-model comparison conducted under identical test conditions to ensure fairness among different methods. It should be noted that these metrics are retained only for comparative purposes in **Table 3**, while the final optimized model—after hyperparameter tuning and retraining—achieves unified performance of MRE = 0.23, MAE = 0.05, RMSE = 0.065, and coefficient of determination $R^2 = 0.95$ on the test set. This clarification highlights that **Table 3** represents benchmarking across models, whereas the latter values reflect the final accuracy of the proposed framework.

Model	MRE	MAE	RMSE
Random forest	0.48	0.062	0.089
Gradient boosting decision tree	0.44	0.054	0.081
XGBoost	0.41	0.049	0.075
Temporal convolutional network	0.36	0.043	0.067
Cox + LSTM (proposed)	0.32	0.037	0.055

Table 3—Comparative performance of different models.

To enhance the performance of the pretrained model, we systematically optimized the hyperparameters using a grid search strategy combined with tenfold cross-validation to ensure that the data set was fully utilized. Each candidate value of window length, learning rate, and number of neurons was fully combined in an orthogonal experimental design, which allowed the independent effect of each hyperparameter to be assessed while maintaining comparability across configurations. Specifically, the window length was varied between 10 and 30 with a step of 10, a range selected to capture short-term transients while avoiding overly long sequences that could dilute precursor signals and increase computational cost. The learning rate was varied between 0.01 and 0.1 with a step of 0.01, and the number of neurons between 64 and 512 with a step of 64. The number of layers was kept the same as in the pretrained model and was not included in the search space, as preliminary experiments showed that this configuration provided stable performance. Due to space limitations, only representative results from the full search space are listed in **Table 4**.

Window Length	Learning Rate	Number of Neurons	MRE	MAE	RMSE
20	0.01	256	0.17	0.03	0.043
20	0.01	128	0.27	0.033	0.048
15	0.02	128	0.30	0.034	0.049
15	0.02	64	0.49	0.039	0.066
10	0.03	64	0.58	0.040	0.068

Table 4—Performance comparison of different parameters of the LSTM model.

The analysis indicates that learning rate has the strongest influence on model performance: Excessively large values cause unstable convergence, while excessively small values lead to slow convergence and underfitting. The number of neurons also plays a substantial role, as too few neurons reduce model capacity while too many increase the risk of overfitting. Window length shows a relatively moderate impact, with the best performance observed at 20. Based on these findings, the final optimal parameters were determined to be a window length of 20, a learning rate of 0.01, and 256 neurons. After hyperparameter tuning, the final model was retrained using the entire data set to maximize the use of available information, and the test set was reserved only for performance reporting.

The resulting prediction accuracy is shown in **Fig. 13**. The graph indicates that the prediction error for both the training and test samples is small, and the predicted production is concentrated near the diagonal. Slightly greater dispersion appears at longer lifespans, mainly due to limited samples in the extreme range and time-dependent operating changes such as reservoir decline or interventions that cannot be fully anticipated. Wells with very short lifespans (<100 days) are often linked to commissioning issues, electrical defects, or adverse fluid conditions, whereas unusually long lifespans (>2,000 days) reflect stable reservoir inflow, appropriate pump sizing, and favorable operating environments. The model achieves an $R^2 = 0.95$ and a mean absolute percentage error (MAPE) of 3.8%, indicating that the combined approach provides highly accurate and reliable predictions of ESP lifespan.

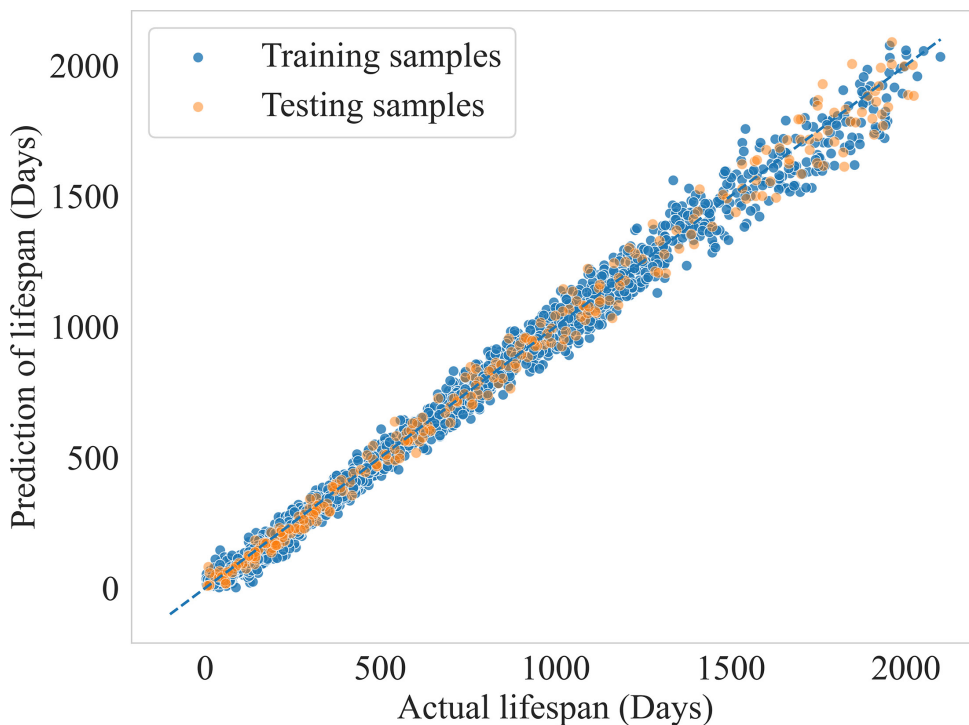


Fig. 13—Lifespan prediction results for training and testing samples, showing predictions closely aligned with actual values ($R^2 = 0.95$, MAPE = 3.8%).

In terms of update frequency, the prediction model is periodically retrained with new production and monitoring data every 30 days to capture gradual changes in reservoir and equipment conditions. In addition, abnormal operating signals—such as sudden changes in current, pressure, or vibration—can trigger an earlier update of the model to ensure robustness under unexpected events. This hybrid strategy balances computational efficiency with responsiveness to dynamic field conditions.

Optimization Method of ESP Operation Regime. The initial optimization framework was designed as a single-objective problem, aiming to maximize the remaining useful life (RUL) of the ESP system based on survival analysis. The predicted lifespan was derived from a hazard function constructed using operating parameters and health indicators. However, optimizing lifespan alone may lead to overly conservative operating conditions that significantly reduce production output, which is unfavorable in real-field applications.

To overcome the limitation of single-objective optimization, which focuses solely on extending the system's lifespan, the framework is extended to a multiobjective approach that incorporates production performance as an additional optimization target. This extension necessitates an accurate estimation of oil production under varying operating conditions, ensuring that both objectives—lifespan and productivity—can be evaluated quantitatively within the same optimization process. To achieve this, a data-driven model is constructed

to map ESP operating parameters to oil production output. The LSTM architecture introduced earlier for temporal modeling is adopted to capture the dynamic relationship between parameters such as frequency, current, intake pressure, and motor temperature, and the corresponding production rate. As a purely data-driven approach, this model does not explicitly represent wellbore and hydrodynamic mechanisms, which may limit absolute accuracy. Nevertheless, it can capture production trends under different operating regimes, providing sufficient guidance for the subsequent multiobjective optimization algorithm. The model is trained on historical production data and validated on a test set. It demonstrates high predictive accuracy, achieving an $R^2 = 0.93$ and a MAPE of 4.5%. The prediction performance of the model is illustrated in **Fig. 14**.

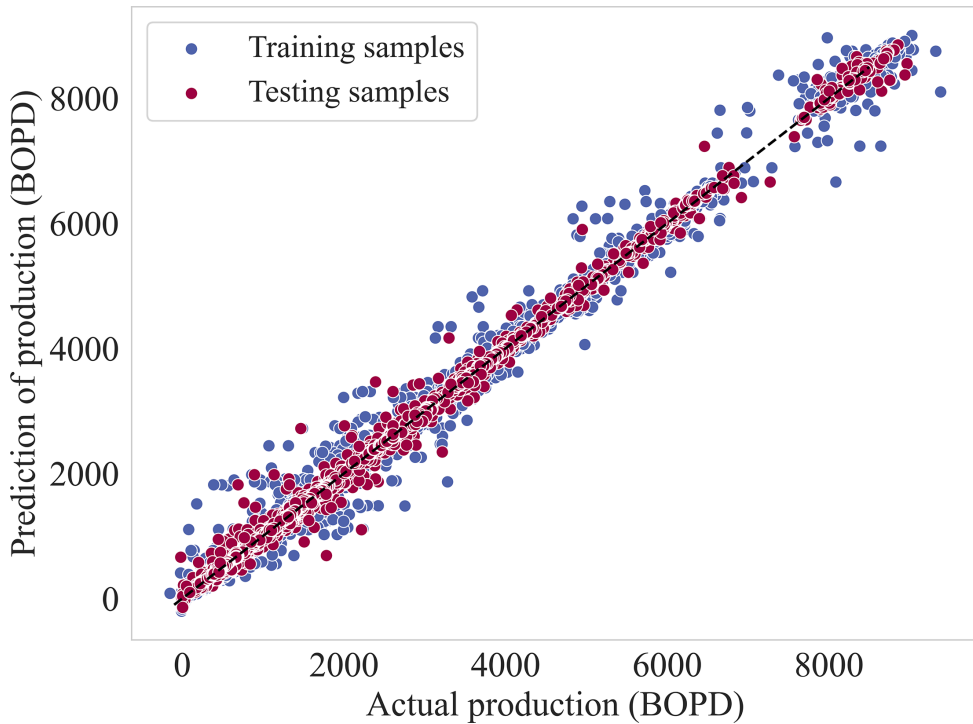


Fig. 14—Production prediction results for training and testing samples, showing high alignment with actual production values ($R^2 = 0.93$, MAPE = 4.5%).

To solve the proposed multiobjective optimization problem involving ESP lifespan and oil production, the NSGA-II algorithm is adopted. NSGA-II is a well-established evolutionary algorithm for handling multiobjective problems without the need for scalarization or predefined weights. It produces a set of Pareto-optimal solutions in a single run, allowing decision-makers to assess trade-offs between conflicting goals. The algorithm evolves a population of candidate solutions through selection, crossover, and mutation and ranks them by Pareto dominance. A crowding-distance mechanism ensures diversity within each front and maintains a well-distributed Pareto frontier. NSGA-II is suitable for this application because ESP operation involves competing goals, specifically maximizing lifespan and production. For instance, high-frequency operation may boost short-term output but accelerate equipment wear, reducing system longevity.

To effectively apply NSGA-II in this context, the multiobjective optimization problem must first be formally formulated by specifying the decision variables, objective functions, and relevant constraints. The mathematical formulation is presented as follows:

$$\left\{ \begin{array}{l} \max \{Lifespan[V_L, s(t, X)], Production(V_P)\} \\ V_L = \{V_1, V_2, \dots, V_{11}\} \\ V_P = \{V_1, V_2, \dots, V_7\} \\ \bar{V} = f(V_1, V_2) \\ \bar{V} = \{V_3, V_4, \dots, V_{11}\} \\ B_1 \leq V_2 \leq B_2 \\ B_3 \leq V_3 \leq B_4 \\ s(t, X) = \exp(-H(t, X)) \end{array} \right. . \quad (12)$$

In Eq. 12, $V_L = \{V_1, V_2, \dots, V_{11}\}$ represents the set of input variables used for lifespan prediction, including productivity index, ESP operating frequency, current, tubinghead pressure, pump intake pressure, pump intake temperature, motor temperature, oil rate, gas rate, liquid rate, and gas/oil ratio. Similarly, $V_P = \{V_1, V_2, \dots, V_7\}$ denotes the subset of variables used in the production prediction model. These parameters comprehensively characterize the operating status of the ESP system and serve as input for the lifespan and production models, respectively. The vector X refers to the set of extracted health-related features (EVs) described earlier, which are used to construct the hazard function for lifespan prediction. The functional relationship $\bar{V} = f(V_1, V_2)$ captures the interaction between operating frequency and system current and is used to determine dependent parameters V_3 through V_{11} . The terms $B_{i,i=1,3}$ and $B_{i,i=2,4}$ denote the lower

and upper bounds for the decision variables, which ensure the operational feasibility and safety of the ESP system. For feasibility handling, the bounds of variable V_2 representing ESP operating frequency are set within [30, 60] Hz, and those of variable V_3 representing motor current are set within [20, 70] A. The survival probability $s(t, X)$ is derived from the hazard function $H(t, X)$, enabling the estimation of remaining useful life under time-varying conditions. The objective functions of lifespan and production are jointly optimized using NSGA-II. The full optimization process is described as follows.

1. Well Productivity Evaluation: Determine the inflow performance relationship curve from well test data and use it to calculate the fluid production index.
2. Operating Point Identification: Determine possible ESP working points by intersecting inflow performance relationship and outflow curves under varying frequencies.
3. Flow Characteristics Calculation: Calculate the wellbore pressure distribution, temperature distribution, and fluid flow rate at the corresponding operating point.
4. Electrical Parameter Estimation: Compute motor power, current, and temperature from the hydraulic load and efficiency to reflect system operating status.
5. NSGA-II Optimization with Embedded Prediction: Use NSGA-II to evolve operating parameters. For each candidate solution, execute Steps 1–4 to generate inputs for prediction models. Compute the survival probability from the hazard function $H(t, X)$ and use it to estimate lifespan. In parallel, use the LSTM model to predict oil production. Evaluate both objectives in each generation. If convergence is not reached, repeat this step.
6. Pareto Front Analysis and Decision Selection: Upon convergence, analyze the Pareto front and select an optimal regime based on trade-offs between lifespan and production.

To support this step, NSGA-II was run with a population size of 200 and 500 generations. Constraints such as pump frequency and motor current limits were handled through a feasibility-based strategy, prioritizing feasible solutions and penalizing infeasible ones. This configuration ensured that the Pareto-optimal results remained both computationally efficient and operationally practical.

Unlike weighted-sum methods that require predefined weights, NSGA-II generates a set of Pareto-optimal solutions that represent different trade-offs between lifespan and production. This allows the optimization process to adaptively adjust operating points according to field requirements. In offshore oilfields with high workover costs, the algorithm naturally emphasizes lifespan, whereas in projects with urgent production goals, it shifts toward higher output.

Adaptivity is achieved through a simple rule that compares the “lifespan pressure” with the “production incentive”:

$$\begin{aligned} C_{\text{workover}}(1 - A) > kP_{\text{oil}}D &\Rightarrow \text{system shifts toward a production-oriented solution;} \\ C_{\text{workover}}(1 - A) \leq kP_{\text{oil}}D &\Rightarrow \text{system shifts toward a lifespan-oriented solution.} \end{aligned} \quad (13)$$

Here, C_{workover} denotes the workover cost, P_{oil} is the oil price, and k is a dimensionless scaling factor (default $k = 1$) used to balance the relative influence of the two terms; its value can be adjusted according to field experience or sensitivity analysis. The term A is defined as follows:

$$A = \min \left(1, \frac{\hat{L}}{H} \right), \quad (14)$$

where \hat{L} is the predicted remaining lifespan and H is the prediction window (e.g., 30 days or 90 days). The term D is expressed as follows:

$$D = \max \left(0, \left(Q_{\text{target}} - \hat{Q} \right) / Q_{\text{target}} \right), \quad (15)$$

where Q_{target} is the production target and Q is the predicted production.

A larger C_{workover} or smaller A increases the lifespan pressure and shifts the decision toward lifespan-oriented solutions. Conversely, higher P_{oil} or larger D strengthens the production incentive and shifts the decision toward production-oriented solutions. The scaling factor k adjusts the balance between the two sides, with $k > 1$ favoring lifespan and $k < 1$ favoring production.

In Step 3, the flow characteristics, including the wellbore temperature and pressure distribution and flow rate, can be calculated with reference to the Beggs-Brill method. In Step 4, the ESP operating current can be calculated using the following equation:

$$I = \frac{P_{\text{SEM}}}{\sqrt{3} \cdot U_{\text{SEMnp}} \cdot \frac{f}{f_{\text{np}}} \cdot \cos\varphi_{\text{SEM}}}, \quad (16)$$

where P_{SEM} is the SEM active power in (kW), U_{SEMnp} is the SEM nameplate voltage (kV), f is the ESP operating frequency (Hz), f_{np} is the nameplate frequency (Hz), and $\cos\varphi_{\text{SEM}}$ is the SEM power factor (p.u.).

For engineering deployment, the framework has been integrated with the SCADA(Supervisory Control and Data Acquisition) system. Real-time well data are collected and preprocessed and then used by prediction models to estimate ESP lifespan and production. The NSGA-II algorithm generates a Pareto set of operating regimes, from which an adaptive rule selects the most suitable solution. The selected parameters are converted into control instructions—such as pump frequency, motor speed, or valve opening—and transmitted to the field system, forming a closed-loop workflow from data acquisition to operational execution.

In addition, the framework incorporates both survival and production models, enabling accurate estimation of ESP performance under varying operating conditions. Unlike fixed empirical methods, this adaptive approach is applicable across different equipment types and reservoir conditions, dynamically adjusting pump operation as fluid properties change. By optimizing for both lifespan and production in real time, the method improves pump efficiency, extends service life, sustains oil output, and enhances overall stability and economic performance, making it well-suited for intelligent oilfield management.

Results and Discussion

Maintenance Strategy for the ESP System. The offshore oil field used for this study has a complicated geological structure, making it challenging to develop. The field heavily relies on the ESP system to produce oil and gas. Due to its offshore location, ESP wells require

expensive workover. To address this issue, we conducted a survival analysis using data from 712 ESP wells in the offshore oil field in China. The analysis resulted in the development of a lifespan prediction model and an ESP operating regime optimization method.

According to the HR obtained from the survival analysis, seven out of the top 10 EVs that had an adverse effect on the ESP production system were associated with SEM. This implies that the operational condition of SEM mainly impacts the lifespan of the ESP system, which can be demonstrated by the proportion of causes of failure at the oilfield site. **Fig. 15** illustrates the percentage of ESP system failure causes at an oilfield site. Within the offshore oil field mentioned above, system failures were found to be caused by SEM in 36.85% of cases, cables in 24.94%, and ESP in only 38.21%. Currently, traditional ESP system maintenance places more emphasis on the upkeep of ESP, whereas it is crucial to prioritize SEM maintenance. These findings are consistent with the optimization results, where lifespan-oriented solutions emphasized thermal stability and motor load balance. By aligning maintenance practices with optimization outputs, the monitoring of SEM-related parameters (e.g., motor temperature, current stability) can be translated into actionable field measures, such as adjusting operating frequency when abnormal patterns occur or scheduling preventive interventions before critical thresholds are exceeded.

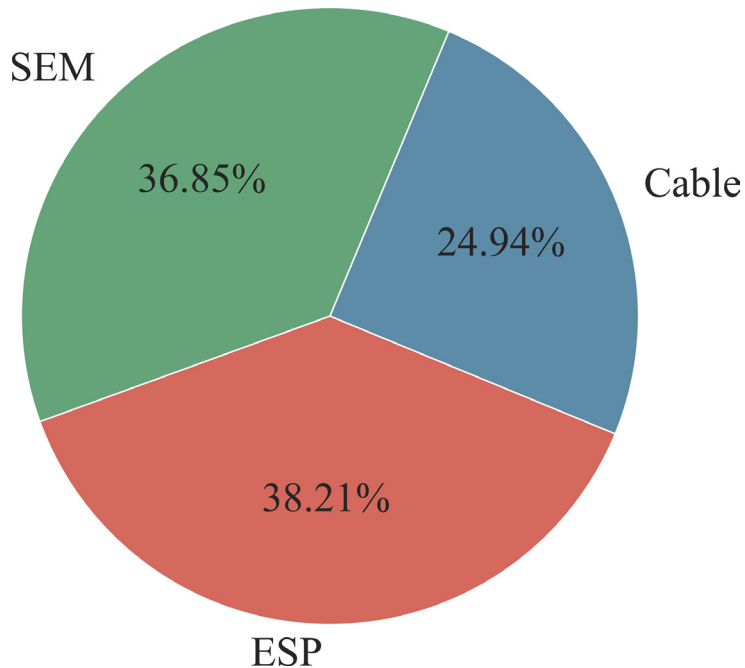


Fig. 15—Percentage distribution of ESP system failure causes at an offshore oil field, showing that failures are mainly attributed to ESP (38.21%) and SEM (36.85%), with cables accounting for 24.94%.

Additionally, when it comes to EVs related to SEM, the std of motor temperature has the most detrimental impact on ESP's lifespan. Fluctuations in temperature can cause thermal stresses between various materials in the SEM, particularly if these materials have varying coefficients of thermal expansion. These frequent temperature changes can result in continual expansion and contraction of the materials, leading to material fatigue and potentially causing cracking. This can ultimately impact the SEM's structural integrity and long-term dependability. In addition, temperature fluctuations affect the lubricant's viscosity, compromising its effectiveness. Unstable temperatures may cause the lubricant to operate at suboptimal levels, increasing the risk of wear and tear over time. Therefore, maintaining stable motor temperatures should be the primary focus of SEM maintenance. To mitigate the impact of varying temperatures on the SEM, it is advisable to use lubricants with versatile temperature adaptability. This guarantees that the internal moving parts of the motor remain lubricated optimally during diverse operating conditions. Additionally, SEM constructed with components possessing lower expansion coefficients can also be used to minimize the impact of temperature fluctuations on the motor's internal structure.

Lifespan Prediction Results of Single Well. In the offshore oil field used for this study, the average lifespan of ESPs is 1,058 days. Half of all ESPs have a lifespan of less than 1,000 days. The distribution of ESP lifespan is illustrated in **Fig. 16**. To prolong the lifespan of ESPs, an accurate prediction of their lifespan is necessary, and the single-well prediction results based on LSTM and survival analysis are shown in **Fig. 17**.

With the use of predictive models rooted in LSTM and survival analysis techniques, precise predictions about lifespan can be made. The results of these predictions have shown that wells with shorter lifespans (e.g., Wells C and D) experienced a significant decline in lifespan at the onset of production. Upon further analysis, it was uncovered that these wells start ESP at a high frequency during the initial stages of production. At the beginning of production, high-frequency, high-intensity operation will accelerate the attrition of ESP and related equipment (such as SEM and protectors), shortening the service life of the equipment. As previously discussed, high-frequency operation can lead to temperature control problems with SEM, increasing the risk of overheating and affecting the reliability and safety of the equipment. Therefore, to prolong lifespan, it is necessary to soft-start the ESP at the start of production.

Operation Regime Optimization Results of Single Well. To evaluate the effectiveness of the multiobjective optimization strategy, in this section we compare the operation regime results of a single well under two distinct optimization objectives, which are maximizing lifespan (single-objective) and jointly optimizing lifespan and cumulative production (multiobjective). **Figs. 18 and 19** illustrate the predicted RUL trajectories alongside the corresponding cumulative production during the optimization period.

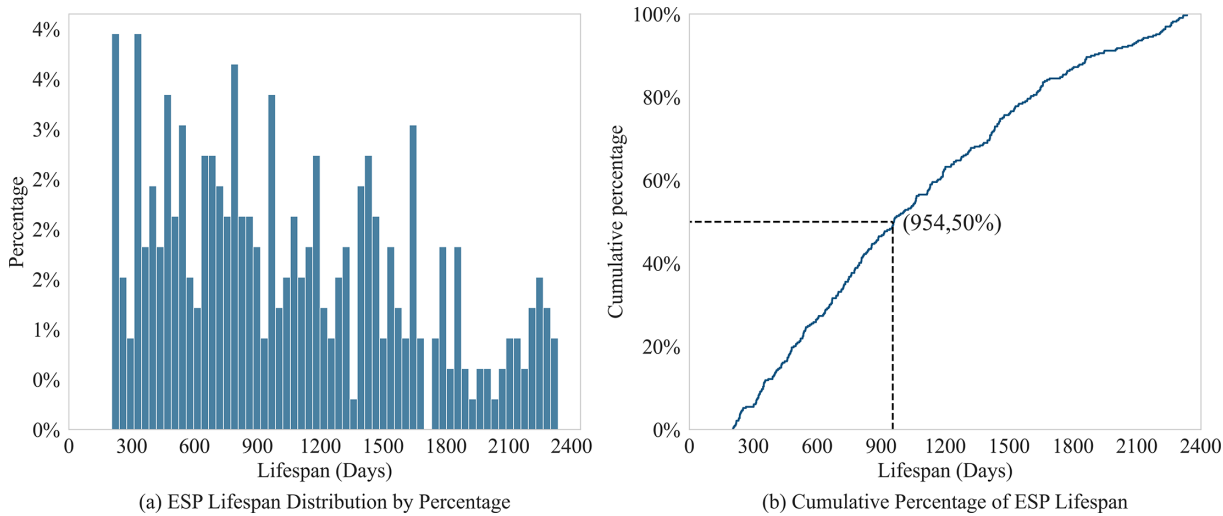


Fig. 16—Distribution and cumulative distribution of ESP lifespans in an offshore oil field: (a) histogram of ESP lifespan distribution by percentage and (b) cumulative percentage of ESP lifespan, showing that half of all ESPs have a lifespan of less than 1,000 days.

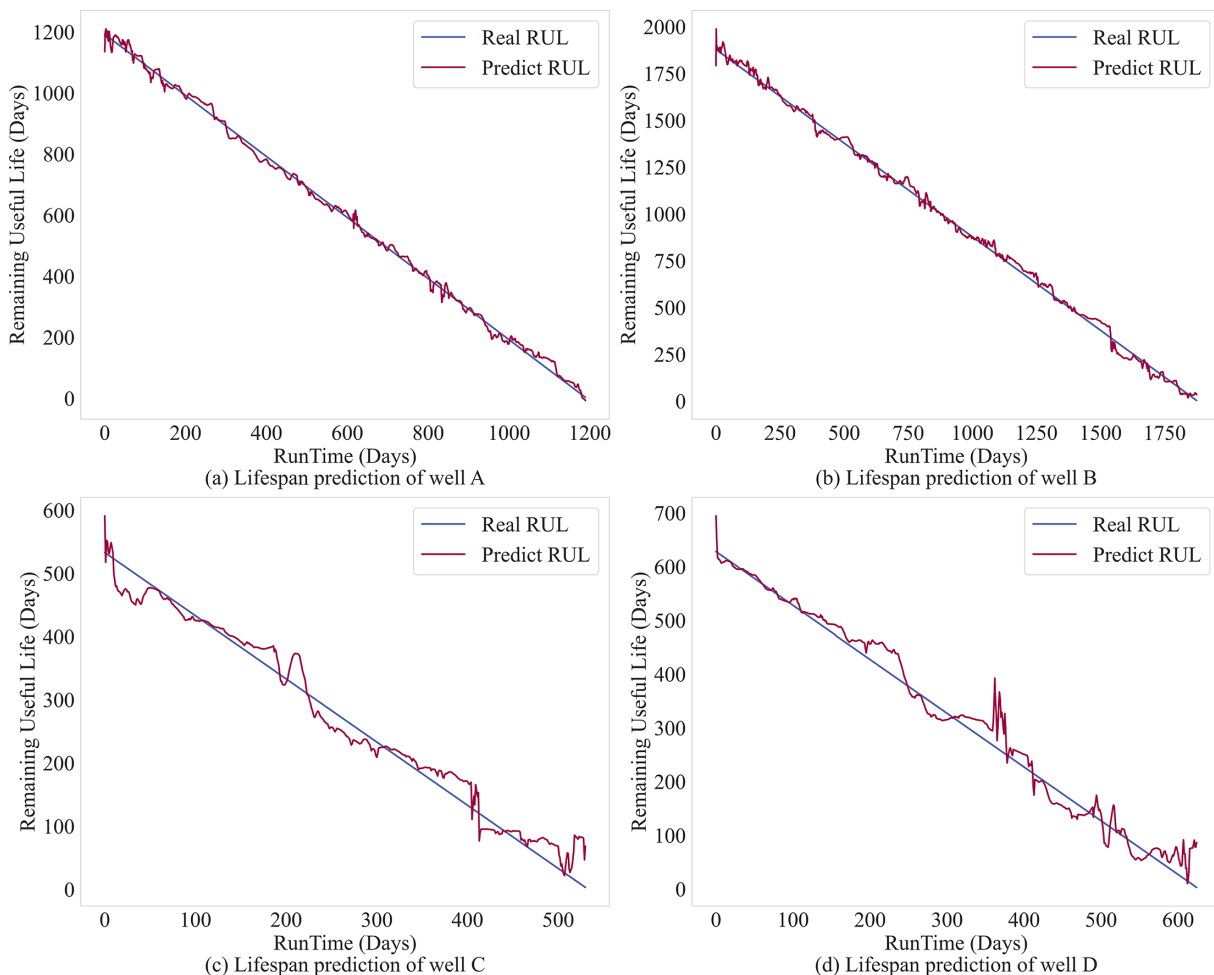


Fig. 17—Single-well lifespan prediction results using LSTM with survival analysis: (a) Well A, (b) Well B, (c) Well C, and (d) Well D, showing good agreement between predicted and actual RUL, with shorter-lived wells exhibiting faster decline at the onset of production.

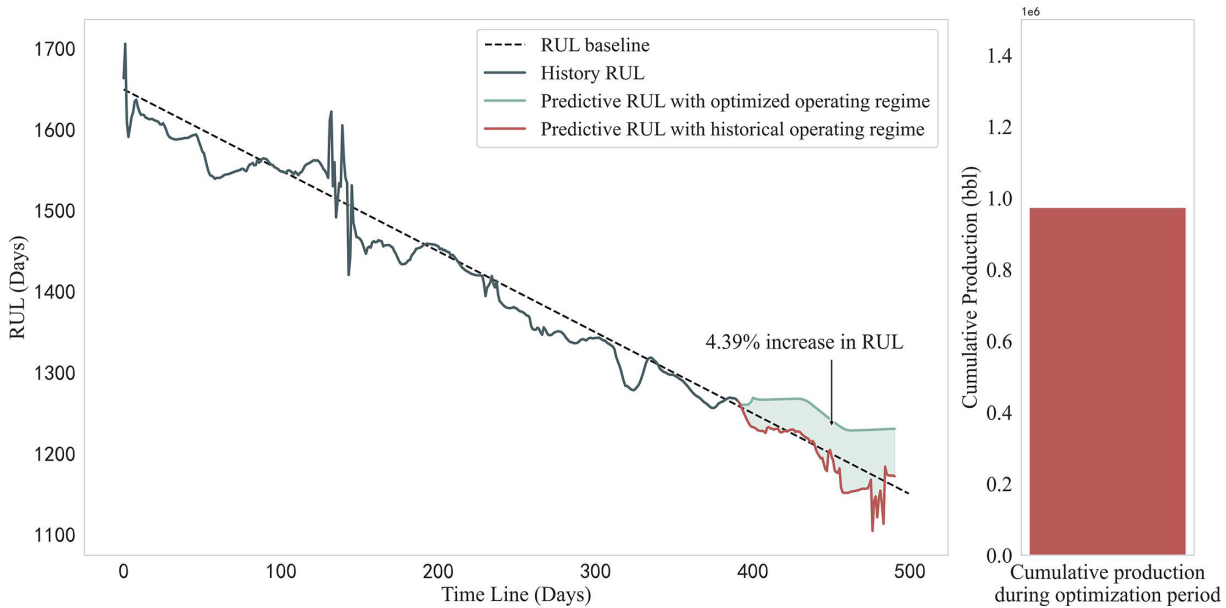


Fig. 18—Operation regime optimization under a single-objective strategy (lifespan maximization), showing a 4.39% increase in RUL but limited cumulative production ($\approx 0.97 \times 10^6$ bbl).

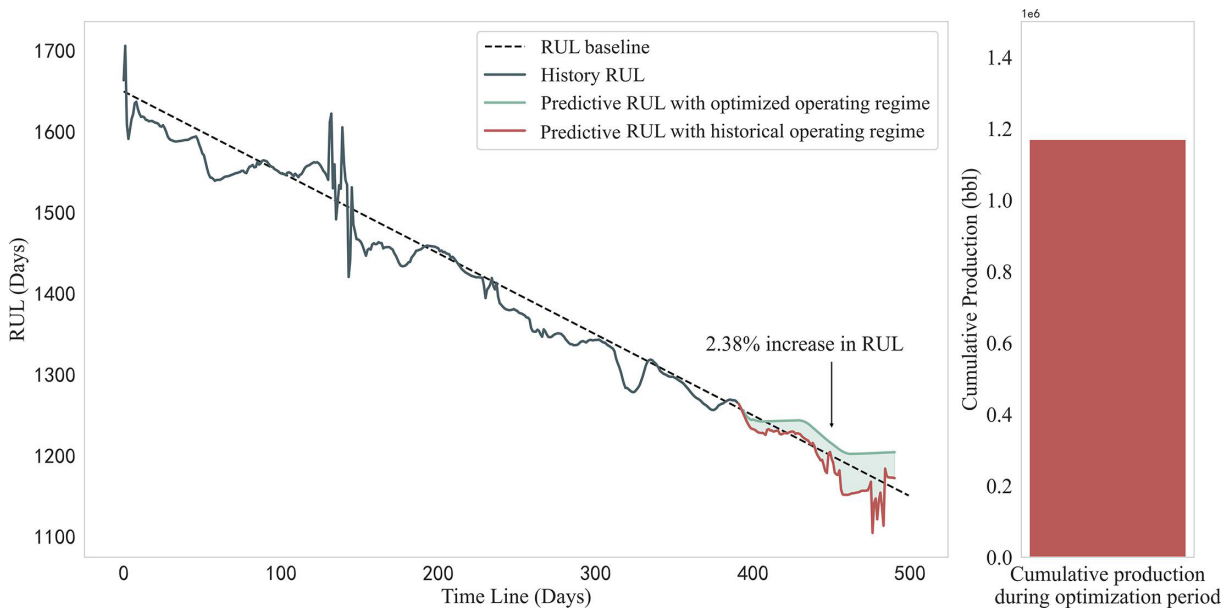


Fig. 19—Operation regime optimization under a multiobjective strategy (lifespan and production), showing a 2.38% increase in RUL with a 20.3% gain in cumulative production ($\approx 1.17 \times 10^6$ bbl).

The improvements in RUL and cumulative production are calculated as relative percentage gains between the optimized and baseline regimes, expressed as follows:

$$\text{Gain (\%)} = \frac{Y_{\text{optimized}} - Y_{\text{baseline}}}{Y_{\text{baseline}}} \times 100, \quad (17)$$

where Y denotes the predicted remaining lifespan or cumulative production over the optimization horizon.

In Fig. 18, the RUL curve under the optimized operating regime shows a 4.39% increase compared with the historical regime. However, the cumulative production during the optimization window reaches approximately 0.97×10^6 bbl. This result reflects the performance under a lifespan-only optimization strategy, which effectively extends the ESP's service time but offers relatively limited production output in the short term. In contrast, Fig. 19 presents the outcome of the multiobjective optimization approach. Although the RUL improvement is relatively modest at 2.38%, the cumulative production increases to approximately 1.17×10^6 bbl, representing a 20.3% increase in production compared with the single-objective optimization.

This result was obtained from field-scale validation involving 30 ESP wells over a 1-year evaluation period. This trade-off highlights the advantage of multiobjective optimization in balancing equipment longevity and production performance. While the lifespan gain is slightly reduced, the improved oil recovery during the ESP's remaining service time provides better economic returns and operational

efficiency. It should be noted that once an optimized strategy is implemented on a well, the counterfactual “nonoptimized” lifespan for the same well can no longer be directly observed. Therefore, the results presented here are based on model-predicted comparisons rather than within-well experimental contrasts.

To further validate the applicability of the method beyond a single-well demonstration, **Table 5** summarizes the original and adjusted operating regimes for 10 representative wells under three optimization strategies. The results confirm consistent trade-offs across multiple wells: Production-priority cases achieve the largest production gains (8–17%) with modest RUL improvements, lifespan-priority cases emphasize RUL extension (up to 6%) with smaller production increases, and balanced strategies provide intermediate benefits in both objectives. These findings reinforce the robustness of the optimization framework under diverse well conditions.

Well ID	Operating Regime	Optimization Strategy	Frequency (Hz)	Current (A)	Pump Inlet Pressure (psi)	Motor Temp (°C)	Predicted Prod. Gain (%)	Predicted RUL Gain (%)
W-01	Original	-	50	60	600	98	-	-
	Adjusted	Balanced	55	65	690	101	8	4
W-02	Original	-	58	68	640	104	-	-
	Adjusted	Production-priority	60	74	760	110	17	2
W-03	Original	-	56	66	620	101	-	-
	Adjusted	Balanced	58	70	710	103	9	4
W-04	Original	-	60	72	680	112	-	-
	Adjusted	Lifespan-priority	52	60	700	100	8	6
W-05	Original	-	51	58	560	105	-	-
	Adjusted	Lifespan-priority	44	50	650	92	8	6
W-06	Original	-	52	64	590	102	-	-
	Adjusted	Lifespan-priority	45	54	620	90	8	5
W-07	Original	-	47	50	570	95	-	-
	Adjusted	Production-priority	55	68	690	101	17	2
W-08	Original	-	54	62	610	100	-	-
	Adjusted	Balanced	57	68	700	103	10	4
W-09	Original	-	46	49	570	96	-	-
	Adjusted	Production-priority	54	66	680	100	17	1
W-10	Original	-	48	47	560	98	-	-
	Adjusted	Balanced	53	56	690	99	10	3

Table 5—Comparison of original and adjusted operating regimes for 10 ESP wells under different optimization strategies, showing key parameter adjustments and predicted improvements in production and RUL.

Building on these case-level comparisons, the overall trade-offs between lifespan and production can be generalized using the Pareto front, as illustrated in **Fig. 20**. Compared with baseline strategies, the Pareto front shifts outward, indicating that higher production can be achieved without significant reduction in lifespan, and vice versa. This outward shift demonstrates the advantage of the proposed approach in balancing durability and productivity at the field scale. Importantly, after applying the optimized operating regimes, the annual average failure rate of ESPs in the studied offshore field decreased from approximately 12% to 8% over a 2-year observation period (2022–2023), based on a cohort of 30 ESP wells. The comparison was made between the year before optimization and the following year under the optimized operating regime, with well type and reservoir conditions held constant, further confirming the practical value and reliability of the framework in real-world deployment.

These results demonstrate that multiobjective optimization offers a more comprehensive and practical solution for field applications, especially under constraints where both asset durability and production targets are critical.

Limitations

While the proposed methodology demonstrates promising results, several limitations should be acknowledged. First, the data set used in this study was obtained from an offshore oil field in China, which has unique geological and operational characteristics. As a result, the generalizability of the survival prediction model and optimization framework to other basins or onshore environments may be limited unless retrained or recalibrated with local field data. Second, the framework relies heavily on the quality and reliability of sensor measurements. Missing data, sensor drift, or measurement noise can reduce prediction accuracy and potentially bias optimization results, although preprocessing techniques such as grey adaptive K-nearest neighbor imputation and outlier filtering were used to mitigate these effects. Third, despite efforts to reduce computational complexity, the integration of Cox survival modeling, LSTM prediction, and NSGA-II optimization requires nontrivial resources. While the inference stage is sufficiently fast for near real-time applications, large-scale deployment across hundreds of wells would demand robust computational infrastructure and efficient task scheduling.

These limitations highlight the need for future research to further validate the framework across diverse reservoir conditions, enhance robustness against sensor uncertainties, and develop lightweight optimization strategies suitable for large-scale field deployment.

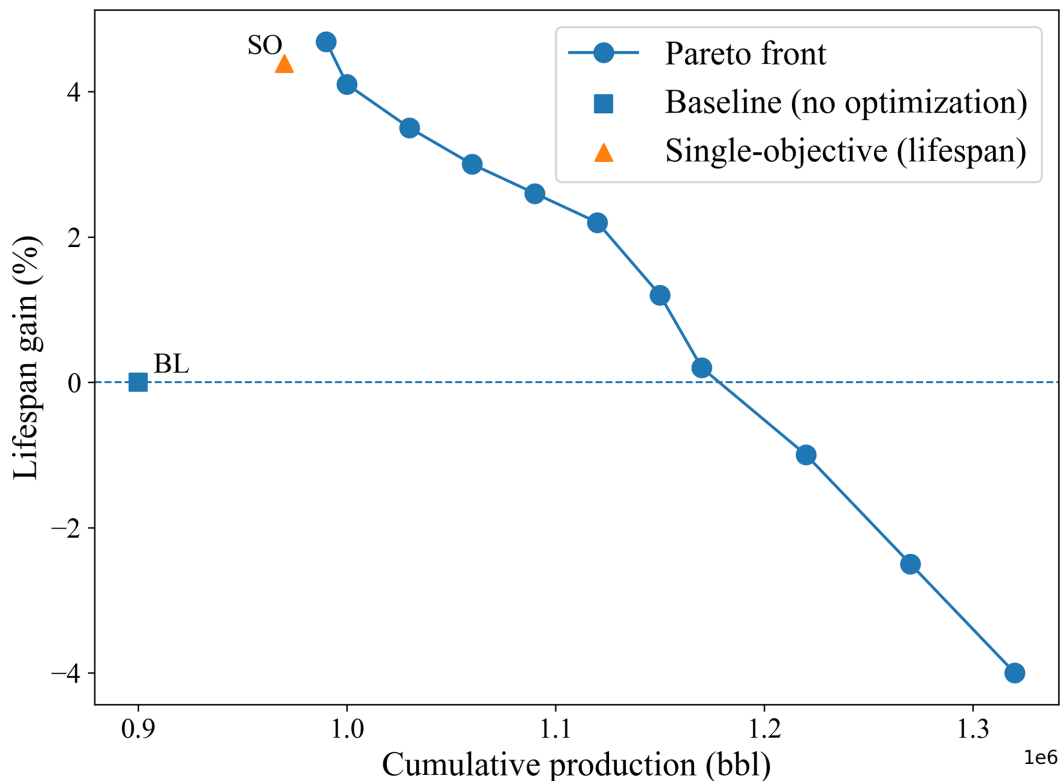


Fig. 20—Pareto front of ESP operation regime optimization obtained using NSGA-II. The horizontal axis shows cumulative production, and the vertical axis shows lifespan gain relative to the baseline. Blue circles represent nondominated solutions forming the Pareto front, the blue square (BL) denotes the baseline without optimization, and the orange triangle (SO) indicates the single-objective lifespan optimization. The outward shift of the Pareto front highlights improved trade-offs between lifespan and production.

Conclusion

Survival analysis identified key parameters affecting ESP lifespan, providing valuable features for prediction and optimization. The proposed framework integrates the CPH model, LSTM network, and NSGA-II optimization, combining statistical interpretability, temporal learning, and adaptive multiobjective decision-making. The model achieved strong accuracy (MRE 0.23, MAE 0.05, RMSE 0.065, and R^2 0.95) and outperformed models without survival-based features. By incorporating survival probability into the optimization, the framework generates Pareto-optimal regimes that explicitly balance lifespan extension and production gain, with field applications showing up to 20.3% higher cumulative production compared with single-objective optimization based on 30 ESP wells monitored over a 1-year period, under comparable lifespan conditions. This approach is adaptable across different equipment combinations and supports dynamic, real-time operation of ESP systems.

Overall, the method provides a novel solution for ESP management, enhancing run life while optimizing trade-offs between productivity and longevity. Future work will validate its transferability to other lift methods and integrate explainable AI to improve transparency and operator trust.

References

- Al Radhi, M., Bermudez, F. A., Al Madhoun, W. et al. 2021. Unlocking the Potential of Electrical Submersible Pumps: The Successful Testing and Deployment of a Real-Time Artificially Intelligent System, for Failure Prediction, Run Life Extension, and Production Optimization. Paper presented at the SPE Symposium: Artificial Intelligence – Towards a Resilient and Efficient Energy Industry, Virtual, 18 October. <https://doi.org/10.2118/208647-MS>.
- Al Sawafi, A., Kazemi, A., Ganat, T. et al. 2024. Developing an ESP Lifespan Predictive Model Using Artificial Intelligence: A Case Study On an Omani Oilfield. Paper presented at the SPE Symposium on Artificial Lift and Production Optimization, Muscat, Oman, 22–24 April. <https://doi.org/10.2118/218601-MS>.
- Alamru, O. A., Pandya, D. A., Warner, O. et al. 2020. ESP Data Analytics: Use of Deep Autoencoders for Intelligent Surveillance of Electric Submersible Pumps. Paper presented at the Offshore Technology Conference, Houston, Texas, USA, 4–7 May. <https://doi.org/10.4043/30468-MS>.
- Al-Ballam, S., Karami, H., and Devegowda, D. 2022. A Data-Based Reliability Analysis of ESP Failures in Oil Production Wells. *J Energ Power Technol* **04** (04): 1–29. <https://doi.org/10.21926/jcpt.2204036>.
- Al-Sadah, H. 2014. ESP Data Analysis to Enhance Electrical Submersible Pump Run Life at Saudi Arabian Fields. Paper presented at the SPE Middle East Artificial Lift Conference and Exhibition, Manama, Bahrain, 26–27 November. <https://doi.org/10.2118/173703-MS>.
- Azmi, P. A. R., Yusoff, M., and Mohd Sallehud-din, M. T. 2024. A Review of Predictive Analytics Models in the Oil and Gas Industries. *Sensors* **24** (12): 4013. <https://doi.org/10.3390/s24124013>.
- Borling, D. C., Sviderskiy, S. V., and Gorlanov, S. F. 2008. “Pumping up the Life” of Electric Submersible Pump Systems, Russian Federation. Paper presented at the SPE Russian Oil and Gas Technical Conference and Exhibition, Moscow, Russia, 28–30 October. <https://doi.org/10.2118/116905-MS>.
- Cox, D. R. 1972. Regression Models and Life-Tables. *J Roy Statist Soc Ser B* **34** (2): 187–202. <https://doi.org/10.1111/j.2517-6161.1972.tb00899.x>.

- Forbicini, F., Pincioli Vago, N. O., and Fraternali, P. 2025. Time Series Analysis in Compressor-Based Machines: A Survey. *Neural Comput Appl* **37** (17): 11001–11038. <https://doi.org/10.1007/s00521-025-11065-0>.
- Klein, J. P. and Moeschberger, M. L. 2003. *Survival Analysis: Techniques for Censored and Truncated Data*. New York, USA: Statistics for Biology and Health, Springer. <https://doi.org/10.1007/b97377>.
- Lee, S., Kim, Y., Choi, H.-J. et al. 2025. Uncertainty-Aware Fault Diagnosis of Rotating Compressors Using Dual-Graph Attention Networks. *Machines* **13** (8): 673. <https://doi.org/10.3390/machines13080673>.
- Melo, R. A. L., Worth, D. J., and Swaffield, S. 2023. Assessment of Real-Time ESP Failure Prediction Using Digital Twin, Machine Learning and Damage Modelling. Paper presented at the SPE Gulf Coast Section - Electric Submersible Pumps Symposium, The Woodlands, Texas, USA, 2–6 October. <https://doi.org/10.2118/214725-MS>.
- Patterson, M. M. 1993. A Model for Estimating the Life of Electrical Submersible Pumps. *SPE Prod & Fac* **8** (04): 247–250. <https://doi.org/10.2118/22790-PA>.
- Peng, L., Feng, L., Guang, Q. et al. 2025. Real-Time ESP Management Framework Using Hybrid Physics-Based and ML Models. Paper presented at the SPE Offshore Europe Conference & Exhibition, Aberdeen, Scotland, UK, 2–5 September. <https://doi.org/10.2118/226795-MS>.
- Pham, S. T., Vo, P. S., and Nguyen, D. N. 2021. Effective Electrical Submersible Pump Management Using Machine Learning. *OJCE* **11** (01): 70–80. <https://doi.org/10.4236/ojce.2021.111005>.
- Sobhy, M. A., Hegazy, G. M., and El-Banbi, A. H. 2025. Dual-Level Electric Submersible Pump (ESP) Failure Classification: A Novel Comprehensive Classification Bridging Failure Modes and Root Cause Analysis. *Energies* **18** (15): 3943. <https://doi.org/10.3390/en18153943>.
- Ture, B. A., Akbulut, A., Zaim, A. H. et al. 2024. Stacking-Based Ensemble Learning for Remaining Useful Life Estimation. *Soft Comput* **28** (2): 1337–1349. <https://doi.org/10.1007/s00500-023-08322-6>.
- Xiao, L., Yang, X., and Yang, X. 2023. A Graph Neural Network-Based Bearing Fault Detection Method. *Sci Rep* **13** (1): 5286. <https://doi.org/10.1038/s41598-023-32369-y>.
- Yang, J., Wang, S., Zheng, C. et al. 2022. Fault Diagnosis Method and Application of ESP Well Based on SPC Rules and Real-Time Data Fusion. *Math Probl Eng* **2022** (July): 1–15. <https://doi.org/10.1155/2022/8497299>.
- Zhu, H., Yu, H., Sun, Q. et al. 2025. Deep Learning-Based Performance Prediction of Electric Submersible Pumps Under Viscous and Gas–Liquid Flow Conditions. *Machines* **13** (2): 135. <https://doi.org/10.3390/machines13020135>.